Published in final edited form as:
Inorg Chem. 2010 April 19; 49(8): 3646–3660. doi:10.1021/ic901550k.

The Role of the Secondary Coordination Sphere in Metal-Mediated Dioxygen Activation

Ryan L. Shook and **A.S. Borovik**
Department of Chemistry, University of California-Irvine, 1102 Natural Sciences II, Irvine, CA 92697-2025

A.S. Borovik: aborovik@uci.edu

Abstract

Alfred Werner proposed nearly 100 years ago that the secondary coordination sphere has a role in determining physical properties of transition metal complexes. We now know that the secondary coordination sphere impacts nearly all aspects of transition metal chemistry, including the reactivity and selectivity in metal-mediated processes. These features are highlighted in the binding and activation of dioxygen by transition metal complexes. There are clear connections between the control of the secondary coordination sphere and the ability of metal complexes to 1) reversibly bind dioxygen or 2) bind and activate dioxygen to form highly reactive M–oxo complexes. In this forum article, several biological and synthetic examples are presented and discussed in terms of structure-function relationships. Particular emphasis is given to systems with defined non-covalent interactions, such as intramolecular hydrogen bonds involving dioxygen-derived ligands. To further illustrate these effects, the homolytic cleavage of C–H bonds by M–oxo complexes with basic oxo ligands is described.

Introduction

In 1912 Alfred Werner advanced the idea that microenvironments surrounding transition metal complexes affect structure and function.[1,2] This new idea invoked the concept that metal complexes can interact with other molecules in specific ways, forming secondary sphere (or outer sphere) species. Until that time, molecular chemistry had developed along the line that the primary coordination sphere was the only contributor to the properties of metal complexes. It is true that essential properties of metal complexes are linked to the primary coordination sphere; however, that alone was not sufficient to explain all of Werner's experimental findings. For instance, the secondary coordination sphere effects were needed in order to explain the association of amines with coordinatively saturated $[M(acac)_3]^n$ complexes and the presence of solvent molecules in crystals of metal complexes. Werner was unaware of the chemical forces acting within the secondary coordination sphere and how they could be utilized to direct chemistry.

Since Werner's seminal insights, the effects of both the primary and secondary coordination spheres have been probed by numerous spectroscopic, analytical, theoretical, and kinetic methods. Fundamental differences are now known to exist between the two coordination spheres, which can be understood within the context of chemical bonding. The primary coordination sphere is dominated by covalent interactions between donor atoms on ligands

Correspondence to: A.S. Borovik, aborovik@uci.edu.

Supporting Information Available: CIF for the X-ray experiment on [Mn^{II}Hbpaa]. This material is available free of charge via the Internet at http://pubs.acs.org.

and metal ions. Experimental and theoretical investigations have provided detailed structure-function relationships that have improved the understanding of key properties, such as correlations between electronic and molecular structures and chemical reactivity, and the development of organometallic catalysts. In contrast, the secondary coordination sphere normally utilizes non-covalent interactions and is associated with determining chemical selectivity.

The growing body of evidence has clearly indicated that control of both spheres is necessary to achieve highly functional complexes. Yet few synthetic systems regulate both the primary and secondary coordination spheres in a predictable manner. The scarcity of such systems can be linked in large part to the secondary coordination sphere and the inability to utilize non-covalent interactions in a reliable and reproducible manner. Because non-covalent bonds are generally weak interactions, they tend to be difficult to control within the secondary coordination sphere, leading to formation of various structures and perturbation of function. These difficulties have led to non-covalent interactions being often overlooked in the design of metal complexes and being relegated to solvation phenomena.[2]

Our thinking about the influences *and usefulness* of the secondary coordination sphere changed with the advent of host-guest chemistry and the emergence of structural metallobiochemistry. The idea that metal complexes could be "recognized" by other molecules via binding to the coordinated ligands (and not the metal centers) was found soon after the realization that host compounds, such as crown ethers, cavitands, and cyptands, could bind anions and small molecules.[3] These findings led to several reports of secondary sphere coordination complexes, examples of which are species formed with crown ethers and metal complexes containing ammine or aquo ligands (Figure 1).[4,5] Note that the *inter*molecular forces used to form these host-guest species are hydrogen bonds (H-bonds).

The breakthrough in spectroscopic and X-ray diffraction analysis of metalloproteins is arguably the most important advance in understanding how to integrate the primary and secondary coordination sphere in inorganic chemistry. Information obtained from these studies illustrate in striking clarity that control of both the primary and secondary coordination spheres can be accomplished in an *intramolecular* manner. Protein active sites have numerous architectural features which aid in regulating function, including 1) metal binding sites utilizing endogenous ligands from amino acid side-chains to regulate the primary coordination spheres; 2) site isolation (when necessary) to avoid unwanted metal ion–metal ion interactions; 3) channels or paths to allow external reagents access to the functionally vital metal center(s); and 4) control of the secondary coordination sphere through protein-derived architectures. These findings have challenged chemists to design and prepare synthetic systems that control both the primary and secondary coordination spheres. This forum article describes some of the biological and synthetic systems that utilize simultaneous regulation of both spheres to achieve dioxygen binding and activation. In particular, we will examine how intramolecuar hydrogen bonds (H-bonds) in the secondary coordination sphere affect function. Correlations between structure and function will be highlighted, with emphasis on the benefits in regulating the secondary coordination sphere during dioxygen activation.

The Problem: Preventing Unwanted Multi-Metallic Species

Although thermodynamically favorable, dioxygen needs to be associated with other species in order for O–O bond cleavage to occur. The association with other species is a kinetic necessity in order to overcome barriers arising from dioxygen's triplet ground state. Metal complexes have many of the requisite properties to bind and active dioxygen, and thus have been utilized by biological and synthetic systems. The normal binding of dioxygen involves

electron transfer from the metal center(s) to the dioxygen, forming metal-superoxo or -peroxo species. The reduction of dioxygen leads to difficulties for any subsequent chemistry involving metal-O_2 complexes, the most frequent being O–O bond cleavage and formation of metal-oxide compounds. For instance, monomeric M-O_2 complexes (M = Cu, Fe, and Mn) are rare because of the thermodynamic propensity to form multi-metallic complexes containing oxo- and hydroxo-bridged complexes (Figure 2).[6] These species are often are exceedingly stable and do not function as either O_2-carriers or reagents to oxidize substrates.

The Site Isolation Approach

One means to circumvent the formation of these unwanted oxo/hydroxo-bridged species is to physically isolate each metal center to such an extent that dimerization is prevented. Site isolation is best illustrated in the placement of active sites in metalloproteins. Comparisons of various molecular structures show correlations between function and the location of the active sites within the proteins. In general, the active sites in electron transfer and metallo-trafficking proteins (Figure 3A) are found near the molecular surface, an obvious evolutionary benefit for these proteins because of their functional need for these active sites to closely interact with other species. In contrast, the dioxygen-binding proteins hemoglobin and myoglobin (Figure 3B) have active sites somewhat buried within the protein matrix, presumably in part to prevent unwanted metal-metal interactions with neighboring molecules. This is further demonstrated by the cytochrome P450s, a family of monooxygenases with internal active sites.

Not surprisingly, there have been several efforts to design synthetic systems that incorporate site isolation characteristics. However, few have been as successful as metalloproteins in reversibly binding dioxygen or O_2 activation. This is especially true of iron, manganese, and copper complexes, in which dioxygen binding under ambient conditions ultimately leads to species with bridging cores (Figure 2). With this said, there have been some notable examples demonstrating that steric bulk within the secondary coordination sphere can produce important findings. Arguably the best-known example of this approach is the ferrous "picket-fence" porphyrin complex of Collman (Figure 4).[7] The steric bulk in this system comes from four functionalized aryl groups attached at the *meso* positions of the porphyrin ring. One regioisomer has all the bulky amide groups positioned on the same side of the ring, producing a sterically constrained cavity that is suitable for dioxygen binding. Efficient dioxygen binding requires a five-coordinate Fe^{II} center, which is accessible by binding an imidazole ligand to the vacant site on the unhindered side of the complex. Importantly, the cavity is sufficiently confined to prevent formation of six-coordinate, bis-imidazole species. There is enough room to have smaller molecules, such as dioxygen, enter the cavity and bind to the iron center—there are several reports illustrating the reversible binding of dioxygen and other small molecules under ambient conditions. Over the years, Collman has used this system to explore fundamental aspects of dioxygen binding and more recently, elaborated on the design to investigate other multi-metal enzymatic systems, including cytochrome c oxidase.[8]

Incorporating steric bulk into other ligand types has also been instrumental in obtaining stable dioxygen adducts of non-heme complexes. For non-heme iron complexes, only three Fe_2(μ-1,2-peroxo) species have been stable enough to be structurally characterized—two of these are only isolable at temperatures below −20°C.[9] Suzuki developed the other complex using a hindered binucleating ligand containing several appended aryl groups (Figure 5).[9d] The Fe_2(μ-1,2-peroxo) complex with this ligand is prepared at *room temperature* and reversibly binds dioxgyen. An amazing aspect of this system was that removal of the dioxygen from the Fe_2(μ-1,2-peroxo) complex was achieved in boiling acetonitrile, conditions expected to lead to irreversible oxidation to give oxo-bridge species. Two reasons, both involving the aryl groups, were postulated to account for the observed

chemistry. Firstly, the presence of two aryl rings on each imidazole moiety caused a weakening of the Fe–N bonds because of steric repulsions, which in turn affected the iron centers' ability to further reduce the peroxo ligand. Secondly, the aryl rings created a sterically constrained hydrophobic cavity around the metal centers, which allowed entry of dioxygen but not other species, especially other di-iron complexes that would lead to irreversible oxidation.

A similar use of sterically bulky groups was needed to control dioxygen binding in copper systems with $Tp^{R,R'}$ ligands (Tp = hydrotris(3,5-R,R'pyrazolyl)borates). Early work with [$Cu^{I}Tp^{Me,Me}$] systems gave some indications that a Cu-O_2 adduct could be stabilized, but the data were incomplete because of complications from competing side-reactions.[10] Kitajima realized that changing the R-groups to $Tp^{tBu,iPr}$ would provide enough steric limitation to isolate the first Cu–superoxo complex (Figure 6A).[11] Moreover, a change to isopropyl groups at the 3-position of the pyrazole rings led to a relatively stable dimeric copper-peroxo complex, with a μ-η^2:η^2-peroxo dicopper(II) core (Figure 6B).[12] Even though the isopropyl groups did not directly interact with the μ-η^2:η^2-peroxo dicopper(II) core, their presence was clearly important by permitting dimerization but limiting other intermolecular oxidative processes. Note that this η^2:η^2-peroxo dicopper(II) complex was a landmark discovery in synthetic bioinorganic chemistry because it correctly predicted the active site structure of the oxygenated form of the respiratory protein hemocyanin. Furthermore, this series of copper complexes provides an excellent illustration of how incremental adjustments within the secondary coordination can have a major impact on functional aspects of dioxygen binding to transition metal complexes.

More recently bulkier ligand systems have been employed to create larger cavities around metal centers for dioxygen binding. Notable examples are the calix[6]arene ligands of Reinaud that contain various tripodal ligands for the binding of a single metal ion. Application of these systems toward dioxygen activation by copper complexes has been reported.[13]

Hydrogen Bonding Networks

Metalloproteins

Further control of the binding and activation of dioxygen is possible through the use of H-bonds within the secondary coordination sphere. Examples of this approach using *inter*molecular H-bonds have already been discussed in connection with the host-guest chemistry. *Intra*molecular H-bonds are now recognized to also be extremely important to control chemistry occurring at metal centers. Thus, the coupling of the effects of site isolation and H-bonding network, both within the secondary coordination sphere, can be used to impact metal mediated transformations.

The best examples of intramolecular H-bonding networks are from biomolecules. H-bonds have bond strengths ranging from 5 to 15 kcal/mol in the condensed phase, which are generally much weaker than covalent interactions found within the primary spheres.[14] Even though H-bonds are weak interactions, they are essential for the binding of dioxygen in hemoglobins and myoglobins. As depicted in Figure 7A with human hemoglobin, dioxygen binds to the iron centers in these proteins via a covalent Fe-O bond and a H-bond between the distal imidazolyl residue of histidine and the coordinated dioxygen.[15,16] Altering the position of the distal histidine in these proteins has pronounced functional effects, an example of which is the enhanced peroxidase activity observed for myoglobins, whose active sites have been engineered to eliminate bifurcated H-bond formation.[17] Moreover, changes in the H-bond network can influence the O_2 affinity, as found when comparing the hemoglobins from human and parasitic nematode *Ascaris suum* (Figure 7B).[18] Nematodes

normally exist in environments having low dioxygen concentrations, especially when compared to those experienced by humans. Notice that the primary coordination spheres around the iron centers are identical in the two hemoglobins. However, their H-bonding networks differ, which appears to affect the dioxygen binding, causing the nematode hemoglobin to have 10^4 times greater affinity for O_2.

H-bonds formed within the secondary coordination sphere also influence dioxygen activation in a number of iron-heme enzymes. For instance, the function of cytochrome P450s, heme-containing monooxygenases that are ubiquitous in nature, have been linked with a protein-derived H-bond network within the secondary coordination sphere of the iron center (vide infra).[19] In addition, recent structural studies have implicated active site H-bond networks in the function of non-heme halogenases.[20] SyrB2, a non-heme Fe(II)/α-ketoglutarate (αKG)-dependent halogenase, catalyzes the conversion of L-Thr to 4-Cl-L-Thr, a modification that is essential for the antifungal activity of syringomycin E.[21], The proposed mechanism involves Cl^-, αKG, and O_2, and proceeds through an [(Cl)Fe(IV)=O] intermediate (Figure 8). XRD studies on the reduced form of SyrB2 revealed that a Cl^- is coordinated to the Fe(II) center, replacing a carboxylate ligand that is normally found in this class of enzymes.[22] The Fe(II)—Cl distance is unusually long at 2.44 Å,[23] in part because of two intramolecular H-bond involving Cl^- (Figure 8).[24] The functional consequences of these non-covalent interactions await further studies but may assist in the selective transfer of Cl· to substrate.

Synthetic Heme Systems

Introducing similar H-bonding networks into synthetic systems has been challenging. Difficulties occur because of our inability to develop systems that are sufficiently rigid to promote *intra*molecular H-bond formation. The usual situations are that H-bond formation involving metal complexes occurs with other species present in the reaction mixture, leading to *inter*molecular products that do not have the chemical properties to promote the targeted function. To overcome this drawback, synthetic complexes must incorporate rigid frameworks that are positioned proximal to metal centers and contain H-bond donors or acceptors. These types of systems often require multi-step syntheses that are difficult and time intensive.

There have been some impressive examples of H-bonding networks within synthetic complexes. The H-bonding networks in hemoglobins and myogolobins have inspired investigations into the role of H-bonds in binding dioxygen by synthetic heme complexes,[25] all of which contain H-bond donors appended from the meso positions of the porphyrin rings. Collman's picket-fence iron porphyrin is an example of such a system (Figure 4)[26,27] —although placement of the amide groups are not within H-bonding distances, there appears to be a dipole contribution that aids in the stabilization of the dioxygen adduct. The situation found with the picket fence porphyrin complexes highlights a design problem with these systems for producing intramolecular H-bond networks. The *meso*-carbon atoms are the most convenient positions to append H-bond donors/acceptors; however, attachment at these positions places functional groups too far from the metal center to engage in H-bonds. To circumvent this problem, porphyrins have been designed to have rigid groups that "hang-over" the metal centers and thus bring H-bond donors/acceptors within critical distances to form intramolecular H-bonds. Reed's urea/amide appended porphyrins[28] and Chang's use of Kemp's acid appended porphyrins are two of the most prominent examples of this approach.[29] Many of these models show a significant increase in affinity for dioxygen binding over comparable systems lacking H-bond donors. These results are consistent with the idea that intramolecular hydrogen bonds help stabilize an Fe-O_2 adduct. In addition, Nocera has prepared 'Hangman' porphyrins that use xanthane units to position H-bond

donors. In one example he showed that a small network of H-bonds is present around a Fe^{III}—OH unit, in both solution and the solid state (Figure 9).[30]

Other Synthetic Systems

Non-heme systems have also been developed to incorporate functional groups that are capable of forming intramolecular H-bond networks.[31,32] One of the first examples pertinent to dioxygen binding was reported by Kitajima who isolated two isomers of a monomeric Mn(III)-peroxo complex, that differ only by the absence or presence of an intramolecular H-bond (Figure 10A).[33] Butler has reported an intriguing $[V^{V}(\eta^2\text{-}O_2)(O)]$ complex with a single intramolecular H-bond (Figure 10B).[34] By far the most investigated non-heme systems are those containing tripodal ligands. Masuda was the first to show the applicability of these systems using polypyridine tripods containing appended H-bond donors.[35] He has done extensive work in this field and has motivated many workers to explore the effects of intramolecular H-bond networks. For instance, he developed a series of tris(carboxyamido-pyridyl) tripods, in which the hindered amide groups serve as H-bond donors. One of these ligands was used to isolate the first example of a stable Cu^{II}–OOH complex, in which two intramolecular H-bonds are formed between the ligand and the proximal oxygen atom of the hydroperoxide (Figure 10C).[35c] This complex was not generated from dioxygen, rather it was formed using a Cu^{II} precursor complex and hydrogen peroxide. Nevertheless, it is an important contribution to copper-peroxo chemistry and illustrates the usefulness of intramolecular H-bond networks.

We have explored dioxygen binding to manganese(II) complexes with the hybrid tripodal ligands, H_5bupa and H_3bpaa (Schemes 1 and 2). Both ligands utilize the carboxyamidopyridyl moieties introduced by Masuda and at least one other anionic donor from either a deprotonated amide or urea. This design takes advantage of an anionic primary coordination sphere, which should aid in the binding of dioxygen, and H-bonding networks within the secondary coordination sphere to stabilize $M\text{-}O_2$ adducts directly from dioxygen. We have shown that $[Mn^{II}H_2bupa]^-$ reacts with dioxygen to form a peroxo adduct (Scheme 1), which further reacts with aldehydes to afford ketones.[36] These results were the first to show that monomeric Mn–peroxo complexes can synthetically be prepared from a Mn^{II} complex and dioxygen at room temperature.

More recently we have explored similar processes with the neutral complex, $[Mn^{II}Hbpaa]$, which uses a new ligand $[Hbpaa]^{2-}$, whose synthesis is outlined in Scheme 2. The solid-state structure of $[Mn^{II}Hbpaa]$ determined by X-ray diffraction (Figure 11) reveals a six-coordinate complex in a distorted octahedral geometry. Four of the coordination sites are occupied by nitrogen donors from the $[Hbpaa]^{2-}$ ligand. The remaining two positions are occupied with the oxygen atoms from the appended carboxyamido groups, which adopt conformations such that their carbonyl moieties are positioned toward the metal center. The oxygen atoms bind to the Mn^{II} center in different ways, a result of the protonation states of the carboxyamide groups. One is deprotonated resulting in the Mn1–O3 bond distance of 2.047(1) Å, whereas a significantly longer Mn1–O2 bond of 2.247(1) Å is observed for a protonated carboxyamide group.

Treating $[Mn^{II}Hbpaa]$ with excess O_2 at room temperature showed no evidence of oxidation, which we ascribed to the manganese center being coordinatively saturated.[37] However, when the same reaction was repeated in the presence of diphenylhydrazine (DPH), a known H-atom source,[38] a new species was observed, which we propose is a Mn^{III}–peroxo intermediate ($[Mn^{III}H_2bpaa(O_2)]$). Spectroscopic measurements support this assignment: after the addition of dioxygen to $[Mn^{II}Hbpaa]$ a new parallel-mode EPR signal appeared at a g value of 8.15 with a six-line hyperfine splitting pattern with $a = 57.7$ G (Figure 12A). Variable temperature studies indicated that this signal arises from a ground state doublet

with a *D*-value of −2.0(3) cm^{-1} and an E/D of 0.13. In addition the absorbance spectrum measured at room temperature (Figure 12B) has bands at λ_{max} = 590 nm (58 M^{-1} cm^{-1}) and 460 nm (sh):[39] taken together these spectroscopic results are nearly the same as observed for $[Mn^{III}H_3bupa(O_2)]^-$ and are consistent with a monomeric Mn^{III}–peroxo complex. Isotopic labeling experiments also support the formulation of this species as $[Mn^{III}H_2bpaa(O_2)]$. Generation of $[Mn^{III}H_2bpaa(O_2)]$ with $^{16}O_2$ produces a new peak in the FTIR spectrum at 891 cm^{-1} and a strong ion with a mass-to-charge ratio of 633.2 (633.2) in the electrospray ionization mass spectrum—these features shift to 839 cm^{-1} and 637.1 (637.2) when samples are prepared with $^{18}O_2$

$[Mn^{III}H_2bpaa(O_2)]$ has similar reactivity to that reported for other metal-peroxo complexes. For instance, treating $[Mn^{III}H_2bpaa(O_2)]$ with cyclohexanecarboxaldehyde afforded cyclohexanone in 67% yield. We have also found that cyclohexanone is formed when $[Mn^{II}Hbpaa]$ and the substrate are exposed to excess O_2 at room temperature. Presumably formation of the Mn^{III}–peroxo complex precedes product formation, yet at present we have not been able to detect $[Mn^{III}H_2bpaa(O_2)]$ under these reaction conditions.

Dioxygen Activation: Generation of Metal-Oxo Intermediates

The previous sections described approaches to stabilize dioxygen adducts to metal complexes. Closely related to these efforts are investigations into the fate of the M–O_2 adduct, in particular what is produced after the breakage of the O–O bond. This is an especially important question because of the pivotal role oxidation has in industrial and biological processes. The consensus view is that O–O bond cleavage produces high valent metal species, many of which have terminal oxo ligands that directly oxidize substrates. One mechanism often invoked is that for the cytochrome P450s, whereby reduction of dioxygen to a terminal oxoiron species (Compound 1) proceeds through several intermediates via the controlled flow of electrons and protons into the active site. The secondary coordination sphere is instrumental in the activation process, with site isolation and H-bond networks being needed to achieve selective oxidation of substrates. For instance, substrate binding in P450, which initiates the catalytic cycles, often utilizes H-bonds formed between substrate and the amino acids within the active site. H-bonds involving the hydroxy group of a nearby threonine (Thr-252) stabilize the Fe-O_2 moiety (Figure 13A).[40,41] This H-bond also appears to assist in O-O bond cleavage because Thr-252 is essential for the reduction of dioxygen to peroxide during the initial stages of dioxygen activation. Moreover, a H-bond network, created with amino acid residues and structural water molecules near the iron center, provides a pathway for protons to traverse through the active site during turnover.

A similar role has been proposed for H-bonds in the active sites of peroxidases and catalases, where hydrogen bonding to Fe-O_2 is believed to polarize the peroxy group, helping facilitate heterolytic O-O bond cleavage.[42] Moreover, H-bonds are formed to the high valent Fe(IV)=O units that are generated in the catalytic mechanism of iron-heme peroxidase.[43,44] A variety of spectroscopic and low-temperature structural studies on compound I and II of horseradish peroxidases have indicated that the oxo of the ferryl group is H-bonded to amino acid residues in the active site (Figure 13B).[45] This has led to the proposal that peroxidase activity is partially regulated by this H-bonding interaction.

Secondary Coordination Sphere, Synthetic Systems, and Dioxygen Activation

Inspired by the findings from metalloproteins, we sought to develop synthetic systems whereby the activation of dioxygen is controlled, at least in part, by H-bond networks in the secondary coordination sphere.[46] Our objectives were to understand how the H-bonds

affected the metal-mediated activation process and the subsequent dioxygen-derived species produced. To accomplish these goals, we designed a series of tripodal ligands that when bonded to transition metal ions create rigid H-bonding cavities around vacant coordination sites. The rationale behind our ligands has been reported[46d,e] and will only briefly be discussed. The key component in our designs is the urea moieties, which was a logical choice based on the vast literature showing their strong tendency to H-bond both in solution and the solid state. In most other systems, the two NH moieties are actively involved in H-bonding to other functional groups. Our systems use the urea units in a different way because of the need to simultaneously bind a metal ion and create an intramolecular H-bonding network. The design principles are illustrated using the parent symmetrical tripodal compound, tris[(*N*-*tert*-butylureayl)-*N*-ethylene] amine (H_6buea) (Figure 14), in which the αNH groups are deprotonated to form a highly anionic metal ion-binding pocket and the remaining parts of the urea groups form the scaffolding of a cavity. Be aware that the preferred conformation of the urea groups place the α'NH groups within the interior of the cavity, positioning them proximal to the metal center and in the proper location to H-bond with external ligands. In addition, using bulky R-groups off the α'-nitrogen atoms isolates the metal centers and limits unwanted metal-metal interactions.

Our first efforts led to the preparation of monomeric iron(III) and manganese(III) complexes with terminal oxo ligands. These types of complexes had been problematic to isolate because of the strong thermodynamic tendency of these metal ions to form M-(μ-O)-M species. Moreover, there are longstanding theoretical predictions that metal centers with four or more *d*-electrons would not be able to form terminal oxo species, especially if they were high spin complexes (vide infra). Despite these concerns, we were successful in stabilizing and isolating $[M^{III}H_3buea(O)]^{2-}$ directly from the activation of dioxygen (Scheme 3). Isotopic labeling studies confirmed that dioxygen was the source of the oxo ligand; a ν(Fe–O) peak at 671 cm^{-1} was observed for $[Fe^{III}H_3buea(^{16}O)]^{2-}$ which shifted to 645 cm^{-1} in $[Fe^{III}H_3buea(^{18}O)]^{2-}$. Similarly, $[Mn^{III}H_3buea(^{16}O)]^{2-}$ had an ν(Mn–O) of 700 cm^{-1} that moves to 672 cm^{-1} in the ^{18}O-isotopomer.

The molecular structures for the two $[M^{III}H_3buea(O)]^{2-}$ were determined in the solid-state by X-ray diffraction methods to reveal trigonal bipyramidal geometries around the metal centers (Figure 15). The oxo ligand binds in an axial position and resides within the H-bonding cavity formed by the $[H_3buea]^{3-}$ ligand. Distances between heavy atoms are often used to gauge whether H-bonds are present in the solid state. Using this criterion, there is strong metrical evidence for intramolecular H-bonds, with each complex having O1…α'N distances of less than 2.9 Å. Further support came from solid-state FTIR studies that showed a shift to lower energy and broadening of the ν(N–H) peaks compare to H_6buea, features that are indicative of strong H-bonds. Notice that the three urea arms of the $[H_3buea]^{3-}$ are symmetrically distributed around the M^{III}–O units in the solid state, which we proposed also occurs in solution. This premise is supported by the axial EPR spectrum obtained for $[Fe^{III}H_3buea(O)]^{2-}$ ($g_{x,y} = 6.0$, $g_z = 2.0$; E/D = 0), data that is consistent with a complex having C_3 symmetry. Additional magnetic measurements on both complexes indicated that $[Fe^{III}H_3buea(O)]^{2-}$ and $[Mn^{III}H_3buea(O)]^{2-}$ have ground spin states of $S = 5/2$ and $S = 2$, respectively.

At first glance, the high-spin character of these complexes was surprising because most known complexes with terminal oxo ligands are low-spin, a finding that agrees with most bonding schemes. All theories have stipulated that multiple bonds are needed between the oxo ligand and a metal center to prepare stable monomeric oxometal complexes.[47] Pi bonds arise between filled *p*-orbitals on the oxo ligand and vacant *d*-orbitals on the metal ion. Calculations predict that low-spin oxometal complexes having C_{4v} symmetry are isolable for metal ions with less than three *d*-electrons because the initial electrons are housed in a

non-bonding orbital (Figure 16A).[48] More electron-rich systems populate anti-bonding π-orbitals, leading to reactive species. Mayer and Thorn showed that C_3-symmetric oxometal complexes with up to four *d*-electrons are also accessible, again provided that the complexes are low-spin (Figure 16B).[48,49]

The properties associated with $[Fe^{III}H_3buea(O)]^{2-}$ and $[Mn^{III}H_3buea(O)]^{2-}$ clearly do not follow the general principles used to describe other oxometal complexes. We have probed our systems to understand the fundamental properties associated with the M—O unit. A combination of spectroscopic and theoretical studies supports the concept that the intramolecular H-bonding network within the complexes has a significant effect on the overall stability of the complexes. Theory showed that the intramolecular H-bonds in a truncated version of $[Fe^{III}H_3buea(O)]^{2-}$ contributed 25 kcal/mol to the stability of the complex.[50] This stabilization was somewhat offset by a decrease in the Fe—O bond energy by 19 kcal/mol compared to that found in a computer-generated control system that does not contain intramolecular H-bonds (Figure 17). The weakening of the Fe–O interaction $[Fe^{III}H_3buea(O)]^{2-}$ was credited exclusively to a reduction in π-bonds between the iron center and oxo ligand to the extent that there is essentially no multiple bond character present. Thus these findings show that in some cases H-bonds can replace π-bonds to oxometal complexes, a result that can have profound implications in the development of new oxidation catalysts and understanding the functions of metalloproteins. We have argued that it may be possible to tune the properties *and reactivity* of oxometal species via modulation in the H-bond networks within the secondary coordination sphere.[46d–f] For example, adjustments in the M–oxo bond energy, as seen in $[Fe^{III}H_3buea(O)]^{2-}$, could lead to new means of controlling the reactivity and selectivity of oxidation reagents. Moreover, it may be possible to develop structure-function correlations based on the type of H-bonding networks surrounding a M–oxo unit.

Modulating Intramolecular H-Bonding Networks

The possibility that H-bonding networks affect the function of $M–O_2$ and M–oxo complexes has been proposed to occur in metalloproteins, where active site structures and protein function are known.[51] A series of heme proteins nicely illustrate this possibility. Myoglobin, heme oxygenase, and horseradish peroxidase (HRP) all have the same square pyramidal geometries within their primary coordination spheres and form $M\text{-}O_2$ adducts. However myoglobin reversibly binds dioxygen, HRP cleaves the O–O bond to destroy peroxide, while heme oxygenase also breaks the O–O bond but to oxidize the porphyrin ring during heme catabolism. These differences in function could be related to the varied H-bonding networks surrounding the iron centers within their respective active sites.

We have developed systems to examine the effects of varied H-bonding networks on dioxygen activation in synthetic complexes.[52] A straightforward design concept was employed for the metal-containing precursors: a series of four Co^{II} complexes were prepared, with trigonal monopyramidal coordination geometries but tunable H-bond networks within their secondary coordination spheres. The investigation required four ligands, each with a tri-anionic metal binding pocket but differing in the number of H-bond donors. Building on the work we had done on the symmetrical urea-based ligand $[H_3buea]^{3-}$ and its amidate counterpart $[\mathbf{0}]^{3-}$, we prepared the two hybrid ligands $[H_2\mathbf{2}]^{3-}$ and $[H\mathbf{1}]^{3-}$ (Figure 18). Their corresponding Co^{II} complexes were synthesized and characterized to show similar molecular and electronic structures. Yet differences in reactivity with dioxygen were observed throughout the series of complexes.

Treating $[Co^{II}H_3buea]^{-}$ and $[Co^{II}H_2\mathbf{2}]^{-}$ with dioxygen (0.5 equiv) under the same experimental conditions (Figure 18) gave the Co^{III}–OH complexes in yields of greater than 70%. Isotopic labeling studies and spectroscopic measurements confirmed the identity of

these complexes. $[Co^{II}H\mathbf{1}]^{-}$, a complex containing only one H-bond donor, showed no appreciable reactivity with dioxygen under these conditions. Excess dioxygen was needed to initiate a reaction, with the first observable species proposed to be a Co^{II}–superoxo species with an $S = ½$ ground spin state. This complex converted to an intermediate that had spectroscopic properties consistent with a Co^{III}–OH complex, but it was too unstable to isolate in pure form. The final complex in the series, $[Co^{II}\mathbf{0}]^{-}$ contained no H-bond donors and did not react with dioxygen under any conditions. Note that we have ruled out steric constraints of the cavity as the reason for this lack of dioxygen reactivity. We have numerous examples of complexes with $[\mathbf{0}]^{3-}$ being able to form five-coordinate complexes, including $[Co^{II}\mathbf{0}(CN)]^{2-}$, which was isolated and structurally characterized.

The trigonal monopyramidal Co^{II} complexes have different levels of reactivity toward dioxygen despite their nearly identical primary coordination spheres. We have suggested that this difference is caused in large part by the intramolecular H-bond networks within the secondary coordination sphere that assist in the binding of O_2, leading to activation of O_2 and formation of the Co^{III}–OH complexes. The data showed a distinct correlation between the number of H-bonds and O_2 binding/activation. The connection is apparent when comparing the reactivity of $[Co^{II}H_2\mathbf{2}]^{-}$ and $[Co^{II}H\mathbf{1}]^{-}$, both of which are capable of forming intramolecular H-bonds. $[Co^{II}H_2\mathbf{2}^{iPr}]^{-}$, with two H-bond donors, reacts at lower O_2 concentrations compared with $[Co^{II}H\mathbf{1}^{iPr}]^{-}$, which only has the possibility of forming one intramolecular H-bond. An additional H-bond donor in $[Co^{II}H_2\mathbf{2}^{iPr}]^{-}$ would assist in dioxygen binding, the essential first step in metal-mediated O_2 activation. Moreover, $[Co^{II}\mathbf{0}^{iPr}]^{-}$ does not bind dioxygen and is the only complex in the series that is incapable of forming intramolecular H-bonds. Finally, there is a clear relationship between the stability of the Co^{III}–OH complexes and the number of intramolecular H-bond donors. $[Co^{III}H_3buea(OH)]^{-}$, with three H-bond donors, was by far the most stable complex in solution, leading to its crystallization. The other complexes react to such an extent in solution that crystallization was not possible. Two reasons could account for the observed stabilities: 1) increasing the number of H-bonds to the Co^{III}–OH unit would lower its nucleophilicity, rendering it less reactive, and 2) the additional H-bonds with an intramolecular network would rigidify the cavity structure, limiting further reactivity with external species.

The structure-function relationships observed in our Co^{II} complexes support the idea that the activity of a metalloprotein is linked to the H-bond networks within secondary coordination spheres. This relationship is especially pertinent in systems involving O_2 binding and activation. It appears likely that other correlations will be established as more data emerge from both biological and synthetic systems. For example, there are now specific examples of engineered metalloproteins, in which changes in H-bonding networks within active sites affect physical properties and reacitivity.[53] Moreover, other synthetic systems have been reported that show strong links between H-bonds and physical properties, such as redox potentials and pK_a values.

Relationship Between Basicity of Oxo Ligand and Chemical Reactivity

The isolation of $[M^{III}H_3buea(O)]^{2-}$ has led to the formation of related complexes, namely the monomeric $M^{III/II}$–OH complexes, $[M^{III}H_3buea(OH)]^{-}$ and $[M^{II}H_3buea(OH)]^{2-}$, which are stable and have been completely characterized, including their molecular structures by X-ray diffraction. Both iron and manganese hydroxo complexes have comparable trigonal bipyramidal coordination geometries to the parent M–oxo complexes with intramolecular H-bonding networks surrounding the M–OH units. We have also been able to detect $[Mn^{IV}H_3buea(O)]^{-}$, a rare example of a Mn^{IV}–oxo complex. Similar to the M^{III}–oxo complexes, the $M^{III/II}$–OH and Mn^{IV}=O complexes are all high spin. A more completed

description of the preparative details and properties of these complexes has been reviewed recently.[46e,f]

We have used these complexes to investigate C–H cleavage by M–oxo complexes.[46c,54] This type of reaction has a wide variety of chemical and biology applications but is one of the most difficult chemical transformations, mostly because of the high dissociation energies of C–H bonds.[55] In many substrates the homolytic bond dissociation energies are greater than 90 kcal/mol, making them thermodynamically difficult to cleave. Like many researchers, we have turned to biology to gain insights into how to accomplish this transformation. Numerous metalloproteins have evolved that achieve this reaction and most studies suggest that M–oxo species, derived from the activation of dioxygen, are the active species involved in C–H bond cleavage. The oxidation strength of M–oxo complexes is usually expressed in terms of redox potentials, with compounds having higher redox potentials being stronger oxidants. Our M–oxo complexes are also derived from dioxygen and are able to cleave C–H bonds; however, their redox potentials are unusually low for complexes that oxidize substrates. For example, the $[Mn^{IV/III}H_3buea(O)]^{-/2-}$ and $[Mn^{V/IV}H_3buea(O)]^{/-}$ redox couples are at −1.0 V and −0.076 V vs Cp_2Fe^+/Cp_2Fe. Moreover, we were unable to observe the $[Mn^{III/II}H_3buea(O)]^{2-/3-}$ process, suggesting that it is lower than −2.0 V vs Cp_2Fe^+/Cp_2Fe. However, $[Mn^{III}H_3buea(O)]^{2-}$ reacts with substrates containing C–H bond of ~80 kcal/mol and $[Mn^{IV}H_3buea(O)]^-$ cleaves C–H bonds of ~90 kcal/mol.

The findings with Mn–oxo complexes suggested that redox potentials alone were not sufficient to fully explain the observed reactivity. To gain a more detailed understanding of our systems, we adapted the approach pioneered by Mayer to use thermodynamic cycles to evaluate the ability of metal-oxo complexes to homolytically cleave C–H bonds.[56] The basis of this approach is to experimentally evaluate the homolytic O–H bond dissociation energies (BDE_{OH}) of M–OH complexes that are produced after C–H bond homolysis—for this transformation to be thermodynamically achievable, the energy required to cleave the C–H bond must be comparable to that produced in forming a O–H bond. The BDE_{OH} can be obtained from the appropriate experimentally determined one-electron redox potentials and pK_a values (Figure 24), using eq 1. The constant C is included in the analysis to account for the solvation of the hydrogen atom and is dependent on the solvent and reference used to measure the redox potentials.[57]

$$BDE_{OH} = 23.06\, E_{1/2} + 1.37\, pK_a + C \quad (1)$$

The analysis of the BDE_{OH} was readily accomplished because the needed Mn–O(H) complexes had already been prepared and characterized as discussed above. From these studies we found that the oxo ligands in the $Mn^{IV/III}$–oxo complexes were basic, with pK_a values of 28.3 and ~15 for $[Mn^{III}H_3buea(OH)]^-$ and $[Mn^{II}H_3buea(OH)]^{2-}$. Taken together with the measured redox potentials, we obtained a BDE_{OH} of 89 kcal/mol for $[Mn^{III}H_3buea(OH)]^-$ and 77 kcal/mol for $[Mn^{II}H_3buea(OH)]^{2-}$ (Figure 19).[54] It is gratifying to note that these predicted values were in close agreement with what was observed in our reactivity studies between substrates having cleavable C–H bonds and the $Mn^{IV/III}$–oxo complexes.[46c,54]

One of the benefits of these thermodynamic analyses were that they showed the importance that the basicity of the oxo ligand has on C–H bond cleavage. It is clearly evident from our work that the strongly basic character of the oxo groups helped drive the observed reactivity with external substrates. Furthermore, the large difference in basicity for the two Mn–oxo complexes predicted that they should react differently with substrates with differing

acidities. The reactivity with 2,4,6-tri-*tert*-butylphenol illustrated this point: $[Mn^{IV}H_3buea(O)]^-$ homolytically cleaved the O—H bond, producing the phenoxyl radical and $[Mn^{III}H_3buea(OH)]^-$, whereas the more basic $[Mn^{III}H_3buea(O)]^{2-}$ deprotonated the phenol[58] producing the phenolate anion and $[Mn^{III}H_3buea(OH)]^-$.

The formation of this series of Mn–O(H) complexes also aided in a comparative kinetic analysis of the C–H bond cleavage from 9,10-dihydroanthracene (DHA). For $[Mn^{III}H_3buea(O)]^{2-}$ at 20°C a corrected second-order rate constant ($k^{Mn(III)\text{-}O}$)[12,59] of 0.48(4) $M^{-1}s^{-1}$ was determined, which is more than an *order of magnitude larger* than the $k^{Mn(IV)\text{-}O}$ of 0.026(2) $M^{-1}s^{-1}$ found for $[Mn^{IV}H_3buea(O)]^-$. This result is counter to what would have been predicted based on the $BDEs_{OH}$ for the Mn—OH analogs (Figure 19), in which the BDE_{OH} of $[Mn^{III}H_3buea(OH)]^-$ is greater than that for $[Mn^{II}H_3buea(OH)]^{2-}$ by 12 kcal/mol. Insights into this unexpected finding came from the measured kinetic isotope effects of 2.6 and 6.8 found for $[Mn^{III}H_3buea(O)]^{2-}$ and $[Mn^{IV}H_3buea(O)]^-$, respectively. These values indicate that both complexes have primary kinetic isotope effects, yet large disparity in their values suggested the possibility that the complexes might react via different mechanistic paths. This premise was supported by Eyring analysis that found a 35 eu difference in the entropy of activation between the two complexes ($\Delta S^{\ddagger} = -14(6)$ for $[Mn^{III}H_3buea(O)]^{2-}$ and $\Delta S^{\ddagger} = -49(4)$ for $[Mn^{IV}H_3buea(O)]^-$), which had a dominant effect on the rate constants for C–H bond cleavage.

We proposed a mechanistic explanation to explain the above rate data. Our kinetic finding coupled with the large difference of ~15 between pK_a values of DHA and $[Mn^{IV}H_3buea(O)]^-$ suggested these reagents react via a proton-couple electron (PCET) transfer path (Figure 20A).[60] This mechanism involves the coming together of the substrate and Mn^{IV}–oxo complex to form a highly ordered transition state. For $[Mn^{III}H_3buea(O)]^{2-}$ the basicity of the oxo ligand influenced the reaction to such an extent that a two-step mechanism occurs, in which the proton transfer precedes electron transfer (PT-ET). Moreover, the similar pK_a values for $[Mn^{III}H_3buea(OH)]^-$ and DHA (ΔpK_a less than 2) and the primary kinetic isotope effect suggested rate-limiting proton transfer. This mechanistic proposal would also produce a charge-delocalized transition state, leading to less ordered solvent molecules, which agrees with the more positive $\Delta S^{\ddagger}$ value determined for this reaction (Figure 20B).

The mechanistic findings for these two Mn–oxo complexes highlights the contributions of the pK_a (i.e., oxo ligand basicity) on chemical reactivity. Our finding that rate of C–H homolysis is affected by oxo basicity shows that there is another tunable parameter (other than redox potential) that can be used in the development of efficient and durable oxidation catalysts. Furthermore, this concept may help resolve a longstanding issue in biochemistry. The evolutionary benefit of coupling O_2 activation with C–H bond cleavage is well recognized and has been cited as a major factor for the success of aerobic life. However dioxygen-derived, metal-containing species, especially high valent metal–oxo species, exist long enough to do irreversible oxidative damage to a protein active site. One means to prevent such detrimental processes is to couple the redox potentials of the M–oxo species with the basicity of the oxo ligand. The benefit of this effect is shown graphically (Figure 21) for the homolytic cleavage of the C–H bond in methane (BDE_{CH} = 104 kcal/mol). At low pK_a valuses, the redox potentials needed to perform this reaction are too high to sustain function. The metal-oxo center would certainly attack other species within the active sites, such as the side-chains of amino acids. As the pK_a value increases there is a concomitant lowering of the redox potential of the M–oxo species to values that ultimately are compatible with a protein. It is the interplay between these two fundamental properties than may lead to efficient oxidation of substrates within an oxygenase.

Green was the first to suggest the importance of the basicity of the oxo ligand in oxygenases.[61] He has been exploring the intermediates formed during turnover in P450s and proposed that redox potentials of the metal-oxo intermediates are much lower than previously thought, thus limiting oxidative damage. In his model, the lower redox potential in compound I, the competent oxidizing species in P450s (Figure 21), is compensated by the basicity of the oxo ligand in compound II, the one-electron reduced form of compound I. Green further proposed that this type of chemistry is possible because of the thiolate ligation to the iron center, which is supported by resonance Raman studies. Our work described above supports this idea, as do two recent reports on synthetic manganese[62] and iron–oxo[63] systems.

Summary

It has been nearly 100 years since Werner first proposed the significance of the secondary coordination sphere in transition metal complexes. Unbeknownst to Werner were many of the central components that define and control the chemistry associated with this sphere. Some advances have been made in determining the regulatory features for the secondary coordination sphere, as highlighted in this article. We know that secondary coordination spheres are essential for the functions of nearly all metalloproteins and that similar characteristics can be designed into synthetic metal complexes. Its importance is now obvious in the chemistry associated with dioxygen binding and activation, as illustrated with respiratory proteins, oxygenases, and synthetic complexes. Yet with all the progress that has been made, our utilization of the secondary coordination sphere still lags far behind that of the primary sphere, in large part because of our inability to manipulate the non-covalent interactions that are needed within the secondary sphere. Examples from our group and others showed that designing systems with rigid scaffolds allows the positioning of functional groups to promote the formation of intramolecular H-bonds, while at the same time isolating metal centers in a manner similar to what occurs within a protein active site. These principles should be applicable to most chemical systems using transition metal ions and undoubtedly would be beneficial to developing new or improved function.

Experimental Section

General Methods

All reagents were purchased from commercial sources and used as received, unless otherwise noted. Solvents were sparged with argon and dried over columns containing Q-5 and molecular sieves. Potassium hydride (KH), as a 30 % dispersion in mineral oil, was filtered with a medium porosity glass frit and washed 5 times each with pentane and Et_2O. The solid KH was dried under vacuum and stored under an inert atmosphere. 1,2-Diphenylhydrazine was recrystallized from Et_2O, dried under vacuum, and stored under an inert atmosphere. $^{18}O_2$ (99 atom % ^{18}O) was purchased from ICON Isotopes (Summit, NJ). Elemental analysis was accomplished at Robertson Microlit laboratories (Madison, NJ). The synthesis of H_3bpaa and its intermediates were carried out under a dinitrogen atmosphere. The syntheses of metal complexes were conducted in a Vacuum Atmospheres, Co. drybox under an argon atmosphere. *N*-[6-(bromomethyl)-2-pyridyl]pivalamide[64] was prepared according to literature methods with minor variations.

Preparative Methods

***N*-(4-fluorophenyl)-2-bromoacetamide—**A solution of 4-fluoroaniline (5.00 mL, 52.1 mmol) and Et_3N (8.5 mL, 61 mmol) in 50 mL $CH_2Cl_2$was cooled to 0°C with an ice water bath. Bromoacetyl bromide (4.60 mL, 53.0 mmol) was diluted with CH_2Cl_2 (~50 mL) and added dropwise. The solution was brought to room temperature and stirred overnight. The

solution was concentrated under reduced pressure to a solid, dissolved in $CHCl_3$, and washed with 2M HCl (3 × 50 mL), H_2O (1 × 50 mL), and brine (1 × 50 mL). The organic layer was dried over anhydrous sodium sulfate, filtered, and concentrated to a solid under reduced pressure. The solid was triturated with CH_2Cl_2 and dried under vacuum to afford 8.06 g (67%). Mp 132–134 °C; ^{1}H NMR (500 MHz, $CDCl_3$) δ 8.14 (1H, s, N*H*), 7.50 (2H, m, Ar*H*), 7.06 (2H, m, Ar*H*), 4.03 (2H, s, CH_2); ^{13}C NMR (500 MHz, $CDCl_3$) δ 164.7, 159.2, 157.3, 135.0, 121.0, 115.6, 115.4, 30.3; ^{19}F NMR (400 MHz, $CDCl_3$) δ 118.8.

Bis[*N*-(6-pivalamido-2-pyridylmethyl)]benzylamine—A solution of *N*-[6-(bromomethyl)-2-pyridyl]pivalamide (6.11 g, 22.5 mmol), benzylamine (1.2 mL, 11 mmol), and Et_3N (3.5 mL, 25 mmol) in 100 mL THF was refluxed for 63 h. The solution was cooled to room temperature, filtered, and concentrated under reduced pressure to a yellow oil. The product was purified by silica gel column chromatography using 2:3 Hexanes/EtOAc to yield 4.06 g (76%). Mp 97–106 °C; ^{1}H NMR (500 MHz, $CDCl_3$) δ 8.10 (2H, d, *J* = 8.3 Hz, NHAr*H*), 7.98 (2H, s, N*H*), 7.68 (2H, t, *J* = 7.9 Hz, NHAr*H*), 7.39 (2H, d, *J* = 7.5 Hz, NHAr*H*), 7.32 (4H, m, Ar*H*), 7.24 (1H, m, Ar*H*), 3.68 (4H, s, NHArCH_2), 3.67 (2H, s, NCH_2Ar), 1.32 (18H, s, C(CH_3)$_3$); ^{13}C NMR (500 MHz, DMSO) δ 177.5, 158.4, 152.0, 139.1, 139.0, 129.1, 128.8, 127.5, 117.8, 112.9, 59.3, 58.2, 39.8, 27.4.

Bis[*N*-(6-pivalamido-2-pyridylmethyl)]amine—To a solution of bis[*N*-(6-pivalamido-2-pyridylmethyl)]benzylamine (5.54 g, 11.4 mmol) and cyclohexene (33.0 mL, 326 mmol) in 80 mL EtOH was added 20% Pd/C (0.284 g). The suspension was refluxed overnight, cooled to room temperature, and filtered through a pad of Celite. The filtrate was concentrated under reduced pressure to a yellow solid, washed with Et_2O, then dried under vacuum to afford 2.54 g (69%). Mp 127–128 °C; ^{1}H NMR (500 MHz, $CDCl_3$) δ 8.13 (2H, d, *J* = 8.3 Hz, Ar*H*), 7.99 (2H, s, N*H*-Ar), 7.87 (2H, t, *J* = 7.9 Hz, Ar*H*), 7.04 (2H, d, *J* = 7.5 Hz, Ar*H*), 3.86 (4H, s, Ar-CH_2), 1.33 (18H, s, C(CH_3)$_3$); ^{13}C NMR (500 MHz, $CDCl_3$) δ 177.1, 157.8, 151.3, 138.8, 118.2, 112.1, 54.3, 39.9, 27.6.

***N*-[bis(6-pivalamido-2-pyridylmethyl)](*N'*-4-fluorophenylcarbamoyl-methyl) amine (H_3bpaa)—**A mixture of bis[*N*-(6-pivalamido-2-pyridylmethyl)]amine (3.82 g, 9.61 mmol), *N*-(4-fluorophenyl)-2-bromoacetamide (2.23 g, 9.61 mmol), and Et_3N (1.4 mL, 10.0 mmol) in 90 mL of THF was refluxed overnight. The reaction mixture was allowed to cool to rt and the Et_3N·HBr that precipitated from the reaction was removed by filtration. The filtrate was concentrated under reduced pressure to a yellow-orange solid, dissolved in CH_2Cl_2 and washed with H_2O (3 × 100 mL) and brine (1 × 100 mL). The organic layer was dried over anhydrous sodium sulfate, filtered, and concentrated under reduced pressure to a solid. The solid was triturated with Et_2O and dried under vacuum to afford 4.83 g (92%). Mp 64–67 °C; ^{1}H NMR (500 MHz, $CDCl_3$) δ 10.12 (1H, s, N*H*-Ar-F), 8.15 (2H, d, *J* = 8.3 Hz, Ar*H*), 7.88 (2H, s, N*H*-Ar), 7.66 (2H, t, *J* = 7.9 Hz, Ar*H*), 7.51 (2H, m, *H*Ar-F), 7.01 (2H, m, *H*Ar-F), 6.97 (2H, d, *J* = 7.4 Hz, Ar*H*) 3.82 (4H, s, Ar-CH_2), 3.51 (2H, s, CH_2CO), 1.27, (18H, s, C(CH_3)$_3$); ^{13}C NMR (500 MHz, $CDCl_3$) δ117.1, 169.7, 158.4, 156.0, 151.6, 139.0, 134.1, 121.8, 119.1, 115.8, 112.8, 65.9, 60.0, 58.8, 39.8, 27.5, 15.3; HRMS (ES+): Exact mass calcd for $C_{30}H_{37}N_6O_3FNa$ [M + Na], 571.2809. Found 571.2797.

***N*-[bis(6-pivalamido-2-pyridylmethyl)](*N'*-4-fluorophenylcarbamoyl-methyl) aminatomanganate(II) ([Mn^{II}Hbpaa])—**A solution of H_3bpaa (0.147 g, 0.268 mmol) in 5 mL anhydrous DMA was treated with solid KH (0.023 g, 0.573 mmol) under an Ar atmosphere. The mixture was stirred until H_2 evolution ceased. $Mn(OAc)_2$ (0.048 g, 0.272 mmol) was added and allowed to stir an additional 45 min. The mixture was filtered to remove KOAc (0.046 g, 88%) to afford 0.159 g (99%) of the pale yellow product. Mass

calcd for $C_{30}H_{34}FN_6O_3Mn$ [M - H], 600.2. Found 600.2. EPR (⊥-mode, X-band, 4 K): *g*-values: 21.0, 5.6, 3.0, 1.66 1.31.

Preparation of [$Mn^{III}H_2bpaa(O_2)$] via O_2 and 1,2-diphenylhydrazine—A solution of [MnHbpaa] (0.114 g, 0.190 mmol) and 1,2-diphenylhydrazine (0.018 mg, 98 mol) in 4 mL anhydrous DMA was treated with excess dry O_2 and stirred for 10 min. MS (ES−); Mass calcd for $C_{30}H_{35}FN_6O_3Mn^{16}O_2$ [M - H], 633.2. Found 633.2. Mass calcd for $C_{30}H_{35}FN_6O_3Mn^{18}O_2$ [M - H], 637.2. Found 637.1. After treating with H_2O (3 mL), the solution was washed with Et_2O (3 × 3 mL). Concentration of the Et_2O solution gave 16 mg (89%) of orange solid. Analysis by ^1H NMR spectroscopy indicated the solid was azobenzene. Via H_2O_2: A solution of [MnHbpaa] (57 mg, 95 μmol) in 3 mL anhydrous DMSO was treated with H_2O_2 (6 μL, 160 μmol, 71.2% aqueous) and stirred for 5 min. MS (ES−); Mass calcd for $C_{30}H_{35}FN_6O_5Mn$ [M - H], 633.2. Found 633.2. λ_{max} (DMSO, nm (ε, $M^{-1}cm^{-1}$)) 590 nm, 460 nm (sh).

Reaction of [$Mn^{III}Hbpaa(O_2)$] with cyclohexanecarboxaldehyde— [$Mn^{III}Hbpaa(O_2)$] was prepared by the method above and allowed to stir for 10 min. One equiv cyclohexanecarboxaldehyde was added via syringe and allowed to stir an additional 3 hrs. After treating with H_2O (3 mL), the solution was washed with Et_2O (3 × 3 mL). The Et_2O washings were combined in a 10 mL volumetric flask and diluted. The solution was analyzed by GC and the amount of cyclohexanone was determined from calibration curves.

Physical Methods

Electronic absorbance spectra were recorded with a Cary 50 spectrophotometer using a 1.00 mm quartz cuvette. Fourier transform infrared spectra were collected on a Varian 800 Scimitar Series FTIR spectrometer. ^1H NMR and ^{13}C NMR spectra were recorded on a Bruker DRX500 spectrometer. Electron paramagnetic resonance (EPR) spectra were collected using a Bruker EMX spectrometer equipped with an ER041XG microwave bridge, an Oxford Instrument liquid He quartz cryostat, and a dual-mode cavity (ER4116DM) or a Bruker ESP300 spectrometer equipped with an Oxford ESR910 cryostat and a bimodal cavity (Bruker ER4116DM). Mass spectrometry of the Mn complexes was done on a Waters LCT Premier mass spectrometer operated in negative ion electrospray mode. Identification of the organic products was done on a Thermo Trace MS+ GC-MS operated in EI mode. Quantitative GC analysis was done on a Hewlett-Packard 6890 Series gas chromatograph equipped with a HP 7683 Series injector. A calibration plot was established using standard procedures for the quantitative determination of organic products.

Supplementary Material

Refer to Web version on PubMed Central for supplementary material.

Acknowledgments

ACKNOWLEDGMENT is made to the NIH (GM 050781) and the NSF (0738252) for financial support. We are thankful for the numerous co-workers who have contributed to the work presented here from our laboratory, including C. MacBeth, R. Gupta, T. Parsell, M.-Y. Yang, R. Lucas, M. Zart, M. Hendrich, W. Gunderson, and E. Solomon.

References

1. (a) Werner A. Ann Chem. 1912; 386:1–272.(b) A. Werner A. Ber. Dtsch. Chem. Ges. 1912; 45:121–130.
2. Colquhoun HM, Stoddart JF, Williams DJ. Angew. Chem. Int. Ed. 1986; 25:487–507.

3. (a) Pederson CJ. Angew. Chem. Int. Ed. 1988; 27:1021–1027.(b) Cram DJ. Angew. Chem. Int. Ed. 1988; 27:1009–1020.(c) Lehn JM. Angew. Chem. In. Ed. 1988; 27:89–112.
4. Colquhoun HM, Stoddart JF, Williams DK. J. Chem. Soc. Chem. Commun. 1981:849–850.
5. Xianglin J, Zuohua P, Meicheng S, Youqi T, Depei H, Zihou T, Jinqi. Chin. Sci. Bull. 1983; 28:1334.
6. (a) Kurtz DM. Chem. Rev. 1990; 90:585–606.(b) Mirica LM, Ottenwaelder X, Stack TDP. Chem. Rev. 2004; 104:1013–1046. [PubMed: 14871148] (c) Lewis EA, Tolman WB. Chem. Rev. 2004; 104:1047–1076. [PubMed: 14871149] (d) Wu AJ, Penner-Hahn JE, Pecoraro VL. Chem. Rev. 2004; 104:903–938. [PubMed: 14871145]
7. (a) Jameson GB, Molinaro FS, Ibers JA, Collman JP, Brauman JI, Rose E, Suslick KS. J. Am. Chem. Soc. 1978; 100:6769–6770.(b) Collman JP, Brauman JI, Doxsee KM, Halbert TR, Bunnenberg E, Linder RE, LaMar GN, Del Gaudio J, Lang G, Spartalian K. J. Am. Chem. Soc. 1980; 102:4182–4192.(c) Collman JP, Brauman JI, Iverson BL, Sessler JL, Morris RM, Gibson QH. J. Am. Chem. Soc. 1983; 105:3052–3064.(d) Collman JP, Zhang Z, Wong K, Brauman JI. J. Am. Chem. Soc. 1994; 116:6245–6251.(d) Momenteau M, Reed CA. Chem. Rev. 1994; 94:659–698.
8. Collman JP, Boulatov R, Sunderland CJ, Fu L. Chem. Rev. 2004; 104:561–588. [PubMed: 14871135]
9. (a) Dong Y, Yan S, Young VG Jr, Que L Jr. Angew. Chem. Int. Ed. 1996; 108:618–620.(b) Kitajima N, Tamura N, Amagai H, Fukui H, Moro-oka Y, Mizutani Y, Kitagawa T, Mathur R, Heerwegh K, Reed CA, Randall CR, Que L Jr, Tatsumi K. J. Am. Chem. Soc. 1994; 116:9071–9085.(c) Kim K, Lippard SJ. J. Am. Chem. Soc. 1996; 118:4914–4915.(d) Ookkubo T, Sugimoto H, Nagayama T, Masuda H, Sato T, Tanaka Y, Maeda Y, Okawa H, Hayashi Y, Uehara A, Suzuki M. J. Am. Chem. Soc. 1996; 118:701–702.
10. Thompson JS. J. Am. Chem. Soc. 1984; 106:4057–4058.
11. Fujisawa K, Tanaka M, Moro-oka Y, Kitajima N. J. Am. Chem. Soc. 1994; 116:12079–12080.
12. (a) Kitajima N, Fujisawa K, Moro-oka Y. J. Am. Chem. Soc. 1989; 111:8975–8976.(b) Kitajima N, Fujisawa K, Fujimoto C, Moro-oka Y, Hashimoto S, Kitagawa T, Toriumi K, Tatsumi K, Nakamura A. J. Am. Chem. Soc. 1992; 114:1277–1291.
13. (a) Blanchard S, Le Clainche L, Rager M-N, Chansou B, Tuchagues JP, Duprat A, Le Mest Y, Reinaud O. Angew. Chem. Int. Ed. 1998; 37:2732–2735.(b) Rondelez Y, Se´ne`que O, Rager M-N, Duprat AF, Reinaud O. Chem.-Eur. J. 2000; 6:4218–4226. [PubMed: 11128287] (c) Izzet G, Douziech B, Prange´ T, Tomas A, Jabin I, Le Mest Y, Reinaud O. Proc. Natl. Acad. Sci. U.S. A. 2005; 102:6831–6836. [PubMed: 15867151] (b) Izzet G, Zeitouny J, Akdas-Killig H, Frapart Y, Menage S, Douziech B, Jabin I, Le Mest Y, Renaud O. J. Am. Chem. Soc. 2008; 130:9514–9523. [PubMed: 18576623]
14. (a) Elmsley J. Chem. Soc. Rev. 1980; 9:91–124.(b) Etter MC. Acc. Chem. Res. 1990; 23:120–126.
15. (a) Perutz MF, Fermi G, Luisi B, Shaanan B, Liddington RC. Acc. Chem. Res. 1987; 20:309–321. (b) Springer BA, Sligar SG, Olsen JS, Philips GN Jr. Chem. Rev. 1994; 94:699–714.
16. (a) Shaanan B. Nature. 1982; 296:683–684. [PubMed: 7070513] (b) Condon PJ, Royer WE Jr. J. Biol. Chem. 1994; 269:25259–25267. [PubMed: 7929217] (c) Philips SEV, Schoenborn BP. Nature. 1981; 292:81–82. [PubMed: 7278969]
17. Ozaki S, Roach MP, Matsui T, Watanabe Y. Acc. Chem. Res. 2001; 34:818–825. [PubMed: 11601966]
18. Yang J, Kloek aP, Goldberg DE, Matthews FS. Proc. Natl. Acad. Sci. USA. 1995; 92:4224–4228. [PubMed: 7753786]
19. (a) Martinis SA, Atkins WM, Stayton PS, Sligar SG. J. Am. Chem. Soc. 1989; 111:9252–9253.(b) Gerber NC, Sligar SG. J. Am. Chem. Soc. 1992; 114:8742–8743.(c) Schlichting I, Berendzen J, Chu K, Stock AM, Maves SA, Benson DE, Sweet RM, Ringe D, Pestko GA, Sligar SG. Science. 2000; 287:1615–1622. [PubMed: 10698731]
20. For recent reviews on halogenases see: Vaillancourt FH, Yeh E, Vosburg DA, Garneau-Tsodikova S, Walsh CT. Chem. Rev. 2006; 106:3364–3378. [PubMed: 16895332] Blasiak LC, Drennan CL. Acc. Chem. Res. 2008; 42:147–155. [PubMed: 18774824]
21. Vaillancourt FH, Yin J, Walsh CT. Proc. Natl. Acad. Sci. USA. 2005; 102:10111–10116. [PubMed: 16002467]

22. Hegg EL, Que L Jr. Eur. J. Biochem. 1997; 250:625–629. [PubMed: 9461283]
23. Orpen, AG.; Brammer, L.; Allen, FH.; Kennard, O.; Watson, DG.; Taylor, R. International Tables for Crystallography. Wilson, AJC., editor. Vol. Vol. C. Dodrecht/Boston/London: Kluwer Academic Publishers; 1995. p. 707-791.
24. (a) Blasiak LC, Vaillancourt FH, Walsh C, Drennan CL. Nature. 2006; 440:368–371. [PubMed: 16541079] (b) Wong C, Fujimoir DG, Walsh CT, Drennan CL. J. Am. Chem. Soc. 2009; 131:4872–4879. [PubMed: 19281171]
25. Momenteau M, Reed CA. Chem Rev. 1994; 94:659–698. and references therein.
26. (a) Collman JP. Acc. Chem. Res. 1977; 10:265–272.(b) Jameson GB, Drago RS. J. Am. Chem. Soc. 1985; 107:3017–3022.
27. Collman JP, Zhang X, Wong K, Bauman JI. J. Am. Chem. Soc. 1994; 116:6245–6251.
28. Wuenschell GE, Tetreau C, Lavalette D, Reed CA. J. Am. Chem. Soc. 1992; 114:3346–3355.
29. Chang CK, Liang Y, Avilés G, Peng S-M. J. Am. Chem. Soc. 1995; 117:4191–4192.
30. (a) Yeh C-Y, Chang CJ, Nocera DG. J. Am. Chem. Soc. 2001; 123:1513–1514. [PubMed: 11456732] (b) Chang LL, Chang CJ, Nocera DG. Org. Lett. 2003; 5:2421–2424. [PubMed: 12841745]
31. (a) Mareques Rivas JC, de Rosales RTM, Parsons S. Dalton Trans. 2003:2156–2163.(b) Mareques Rivas JC, Salvagni E, de Rosales RTM, Parsons S. Dalton Trans. 2003:3339–3349.(c) Mareques Rivas JC, Prabaharan R, de Rosales RTM. Chem. Commun. 2004:76–77.(d) Mareques Rivas JC, Salvagni E, Parsons S. Chem. Commun. 2004:460–461.(e) Mareques Rivas JC, de Rosales RTM, Parsons S. Chem. Commun. 2004:610–611.(f) Mareques Rivas JC, Prabaharan R, Parsons S. Dalton Trans. 2004:1648–1655. [PubMed: 15252616] (g) Mareques Rivas JC, Prabaharan R, de Rosales RTM, Metteau L, Parsons S. Dalton Trans. 2004:2800–2807. [PubMed: 15514768] (h) Mareques Rivas JC, Salvagni E, Parsons S. Dalton Trans. 2004:4185–4192. [PubMed: 15573171] (i) Feng G, Mareque-Rivas JC, de Rosales RTM, Williams NH. J. Am. Chem. Soc. 2005; 127:13470–13471. [PubMed: 16190690] (j) Feng G, Mareque-Rivas JC, Williams NH. Chem. Commun. 2006:1845–1847.(k) Mareque-Rivas JC, Hinchley SL, Metteau L, Parsons S. Dalton Trans. 2006:2316–2322. [PubMed: 16688319] (l) Metteau L, Parsons S, Mareque-Rivas JC. Inorg. Chem. 2006; 45:6601–6603. [PubMed: 16903713] (m) Feng G, Natale D, Prabaharan R, Mareque-Rivas JC, Williams NH. Angew. Chem. Int. Ed. Engl. 2006; 45:7056–7059. [PubMed: 17009384]
32. (a) Berreau LM, Allred RA, Makowski-Grzyska MM, Arif AM. Chem. Commun. 2000:1423–1424.(b) Berreau LM, Makowska-Grzyska MM, Arif AM. Inorg. Chem. 2001; 40:2212–2213. [PubMed: 11327890]
33. Kitajima N, Komatsuzaki H, Hikichi S, Osawa M, Moro-oka Y. J. Am. Chem. Soc. 1994; 116:11596–11597.
34. Kinblin C, Bu X, Bulter A. Inorg. Chem. 2002; 41:158–160. [PubMed: 11800601]
35. (a) Harata M, Jitsukawa K, Masuda H, Einaga H. Chem. Lett. 1995; 24:61–62.(b) Ogo S, Wada S, Watanabe Y, Iwase M, Wada A, Harata M, Jitsukawa K, Masuda H, Einage H. Angew. Chem. Int. Ed. 1998; 37:2101–2104.(c) Wada A, Harata M, Hasegawa K, Jitsukawa K, Masuda H, Mukai M, Kitagawa T, Einaga H. Angew. Chem. Int. Ed. 1998; 37:798–799.(d) Ogo S, Yamahara R, Roach M, Suenobu T, Aki M, Ogura T, Kitagawa T, Masuda H, Fukuzumi S, Watanabe Y. Inorg. Chem. 2002; 41:5513–5520. [PubMed: 12377047] (e) Yamaguchi S, Wada A, Funahashi Y, Nagatomo S, Kitagawa T, Jitsukawa K, Masuda H. Eur. J. Inorg. Chem. 2003:4378–4386.(g) Wada A, Ogo S, Nagatomo S, Kitagawa T, Watanabe Y, Jitsukawa K, Masuda H. Inorg. Chem. 2002; 41:616–618. [PubMed: 11849054]
36. Shook RL, Gunderson WA, Greaves J, Ziller JW, Hendrich MP, Borovik AS. J. Am. Chem. Soc. 2008; 130:8888–8889. [PubMed: 18570414]
37. [Mn^{II}Hbpaa] also reacts directly with H_2O_2 at room temperature in DMSO to produce [$Mn^{III}H_2$bpaa(O_2)] in nearly quantitative yields.
38. [$Mn^{III}H_2$bpaa(O_2)] was also produced with indene and fluorine as the H-atom sources, whereas no reactions were observed in the presence of 9,10-dihydroanthracene and xanthene.
39. The absorbance spectrum for [$Mn^{III}H_2$bpaa(O_2)] was prepared by treating [Mn^{II}Hbpaa] with H_2O_2 at room temperature. Spectra obtained with dioxygen were similar but contained a strong absorbance from azobenzene.

40. (a) Martinis SA, Atkins WM, Stayton PS, Sligar SG. J. Am. Chem. Soc. 1989; 111:9252–9253.(b) Gerber NC, Sligar SG. J. Am. Chem. Soc. 1992; 114:8742–8743.(c) Sono M, Roach MP, Coulter ED, Dawson JH. Chem Rev. 1996; 96:2841–2887. [PubMed: 11848843]
41. (a) Schlichting I, Berendzen J, Chu K, Stock AM, Maves SA, Benson DE, Sweet RM, Ringe D, Pestko GA, Sligar SG. Science. 2000; 287:1615–1622. [PubMed: 10698731] (b) Nagano S, Poulos TL. J. Biol. Chem. 2005; 280:31659–31663. [PubMed: 15994329]
42. Poulos TL. Adv. Inorg. Biochem. 1988; 7:1–36. [PubMed: 2821744]
43. Mukai M, Nagano S, Tanaka M, Ishimori K, Morishima I, Ogura T, Watanabe Y, Kitagawa T. J. Am. Chem. Soc. 1997; 119:1758–1766. and references therein.
44. (a) Fülöp V, Phizackerley RP, Soltis SM, Clifton IJ, Wakatuski S, Erman J, Hajdu J, Edwards SL. Structure. 1994; 2:201–208. [PubMed: 8069633] (b) Bonagura CA, Bhaskar B, Shimizu H, Li H, Sundaramoorthy M, McRee DE, Goodin DB, Poulos TL. Biochemistry. 2003; 42:5600–5608. [PubMed: 12741816]
45. Berglund GI, Carlsson GH, Smith AT, Szöke H, Henriksen A, Hajdu J. Nature. 2002; 417:463–466. [PubMed: 12024218]
46. Selected references: Hammes BS, Young VG, Borovik AS. Angew. Chem. Int. Ed. 1999; 38:666–669. MacBeth CE, Golombek AP, Young VG Jr, Yang C, Kuczera K, Hendrich MP, Borovik AS. O_2 Science. 2000; 289:938–941. Gupta R, Borovik AS. J. Am. Chem. Soc. 2003; 125:13234–13242. [PubMed: 14570499] MacBeth CE, Gupta R, Mitchell-Koch KR, Young VG, Lushington GH, Thompson WH, Hendrich MP, Borovik AS. J. Am. Chem. Soc. 2004; 126:2556–2567. [PubMed: 14982465] Borovik AS. Acc. Chem. Res. 2005; 38:54–61. [PubMed: 15654737] Shook RL, Borovik AS. Chem. Commun. 2008:6095–6107.
47. (a) Nugent, WA.; Mayer, JM. Metal-Ligand Multiple Bonds: The Chemistry of Transition Metal Complexes Containing Oxo, Nitrido, Imido, Alkylidene, or Alkylidyne Ligands. 1st ed.. New York: Wiley; 1988. (b) (a) Griffith WP. Coord. Chem. Rev. 1970; 5:459–517.(b) Gulliver DJ, Levason W. Chem. Soc. Rev. 1982; 46:1–127.
48. Mayer JM, Thorn DL, Tulip TH. J. Am. Chem. Soc. 1985; 107:7454–7462. and references therein.
49. Selected examples of other oxo complexes with at least 4 d-electrons:[48] Wilkinson G, Hay-Motherwell R, Hussian-Bates B, Hursthouse MB. Polyhedron. 1993; 12:2009–2012. Cheng W-C, Yu W-Y, Cheung K-K, Che C-M. J. Chem. Soc. Dalton Trans. 1994:57–62. Welch TW, Ciftan SA, White PS, Thorp HH. Inorg. Chem. 1997; 36:4812–4821. [PubMed: 11670161] Spaltenstein E, Conry RR, Critchlow SC, Mayer JM. J. Am. Chem. Soc. 1989; 111:8741–8742. Rohde J-U, In J-H, Lim MH, Brennessel WW, Bukowski MR, Stubna A, Münck E, Wam W, Que L Jr. Science. 2003; 299:1037–1039. [PubMed: 12586936] England J, Martinho M, Farquhar ER, Frisch JR, Bominaar EL, Munck E, Que L Jr. Angew. Chem. Int. Ed. 2009; 48:3622–3626.
50. Dey A, Hocking RK, Larsen PL, Borovik AS, Hedman B, Hodgson KO, Solomon EI. J. Am. Chem. Soc. 2006; 128:9825–9833. [PubMed: 16866539]
51. Selected examples: Holmes MA, Stenkamp RE. J. Mol. Biol. 1991; 220:723–737. [PubMed: 1870128] Fülöp V, Phizackerley RP, Soltis SM, Clifton IJ, Wakatuski S, Erman J, Hajdu J, Edwards SL. Structure. 1994; 2:201–208. [PubMed: 8069633] Mukai M, Nagano S, Tanaka M, Ishimori K, Morishima I, Ogura T, Watanabe Y, Kitagawa T. J. Am. Chem. Soc. 1997; 119:1758–1766. and references therein; Dunietz BD, Beachy MD, Cao Y, Whittington DA, Lippard SJ, Friesner RA. J. Am. Chem. Soc. 2000; 122:2828–2839. Gherman BF, Dunietz BD, Whittington DA, Lippard SJ, Friesner RA. J. Am. Chem. Soc. 2001; 123:3836–3837. [PubMed: 11457123] Du Bois J, Mizoguchi TJ, Lippard SJ. Coord. Chem. Rev. 2000; 200–202:443–485. Berglund GI, Carlsson GH, Smith AT, Szöke H, Henriksen A, Hajdu J. Nature. 2002; 417:463–468. [PubMed: 12024218] Tomchick DR, Phan P, Cymborowski M, Minor W, Holman TR. Biochemistry. 2001; 40:7509–7517. [PubMed: 11412104]
52. Lucas RL, Muhkerjee J, Zart MK, Sorrell TN, Powell DR, Borovik AS. J. Am. Chem. Soc. 2006; 128:15476–15489. [PubMed: 17132015]
53. (a) Miller AF. Acc. Chem. Res. 2008; 41:501–510. [PubMed: 18376853] (b) Jackson TA, Brunold TC. Acc. Chem. Res. 2004; 37:461–470. [PubMed: 15260508]
54. Parsell TH, Yang M-Y, Borovik AS. J. Am. Chem. Soc. 2009; 131:2762–2763. [PubMed: 19196005]
55. Stone KL, Borovik AS. Curr. Opin. Chem. Biol. 2009; 13:114–118. [PubMed: 19297238]

56. (a) Mayer, JM. Biomimetic Oxidations Catalyzed by Transition Metal Complexes. Meunier, B., editor. London: Imperial College Press; 2000. p. 1-43.(b) Mayer JM. Annu. Rev. Phys. Chem. 2004; 55:363–390. [PubMed: 15117257]
57. (a) Bordwell FG, Cheng J-P, Ji G-Z, Satish AV, Zhang X. J. Am. Chem. Soc. 1991; 113:9790–9795.(b) Parker VD, Handoo KL, Roness F, Tilset M. J. Am. Chem. Soc. 1991; 113:7493–7498.
58. 2,4,6-tri-*tert*-phenol: BDE_{OH} = 85 kcal/mol, pK_a = 18. Bordwell FG, Zhang X-M. J. Org. Chem. 1995; 8:529–535.
59. The second-order rate constants were normalized for the four reactive C—H bonds per substrate molecule.
60. There have been several discussions in the literature on the proper nomenclature for this process: two of the most common are hydrogen atom transfer (HAT) and proton-coupled electron transfer (PCET). We chose to use the latter in this article. For more detailed discussions see reference 55b and Huynh MHV, Meyer TJ. Chem. Rev. 2007; 107:5004–5064. [PubMed: 17999556]
61. (a) Green MT, Dawson JH, Gray HB. Science. 2004; 304:1653–165. [PubMed: 15192224] (b) Green MT. Curr. Opin. Chem. Biol. 2009; 13:84–88. [PubMed: 19345605]
62. Lansky DE, Goldberg DP. Inorg. Chem. 2006; 45:5119–5125. [PubMed: 16780334]
63. Sastri CV, Lee J, Oh K, Lee YJ, Lee J, Jackson TA, Ray K, Hirao H, Shin W, Halfen JA, Kim J, Que L Jr, Shaik S, Nam W. Proc. Nat. Acad. Sci. 2007; 104:19181–19186. [PubMed: 18048327]
64. Harata M, Hasegawa K, Jitsukawa K, Masuda H, Einaga H. Bull. Chem. Soc. Jpn. 1998; 71:1031–1038.

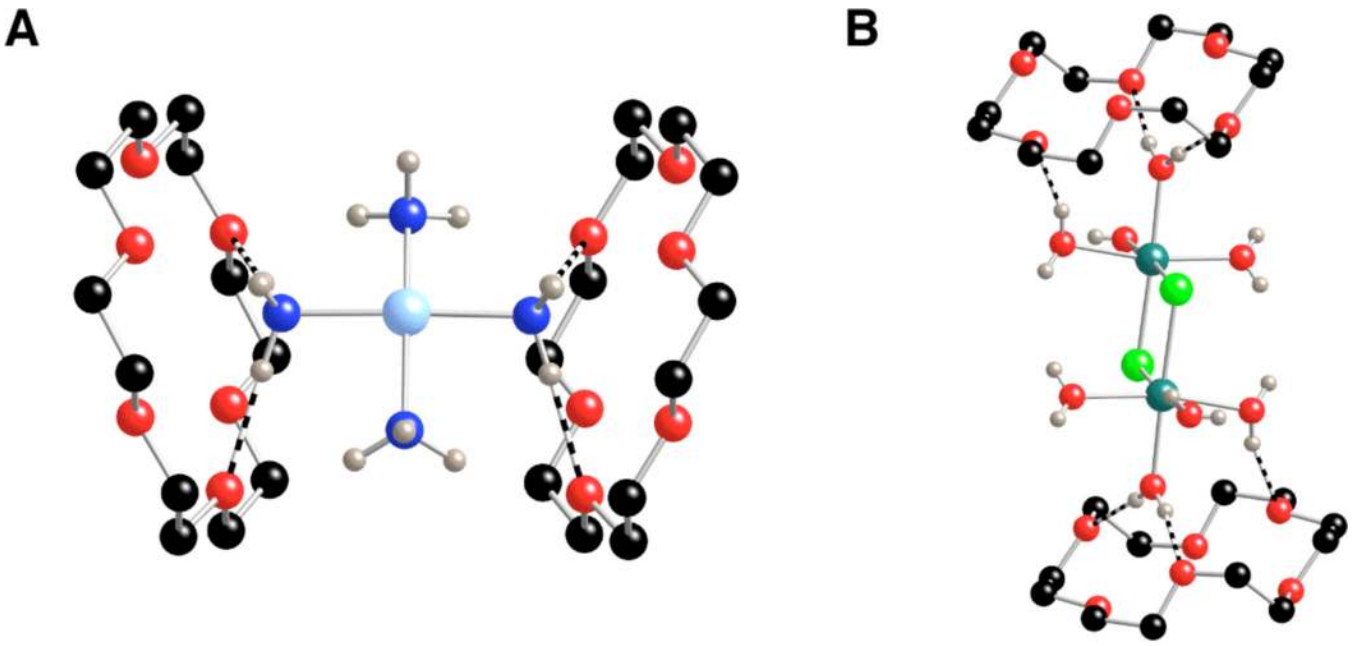

Figure 1.
Two examples of secondary coordination sphere interactions with crystalline lattices: (**A**) 18-crown-6.[$Cu^{II}(NH_3)_4$] and (**B**) 18-crown-6.[$Mn^{II}(H_2O)_4(Cl)_2$]. Only ammine and aquo hydrogen atoms are shown for clarity.

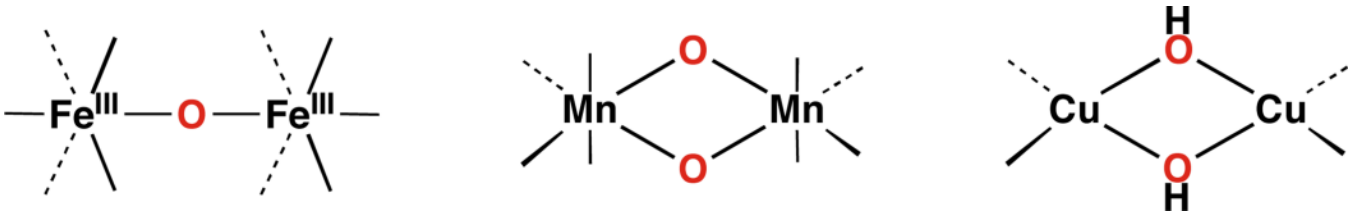

Figure 2.
Common structural motifs that arise from the activation of dioxygen by iron, manganese, and copper complexes.

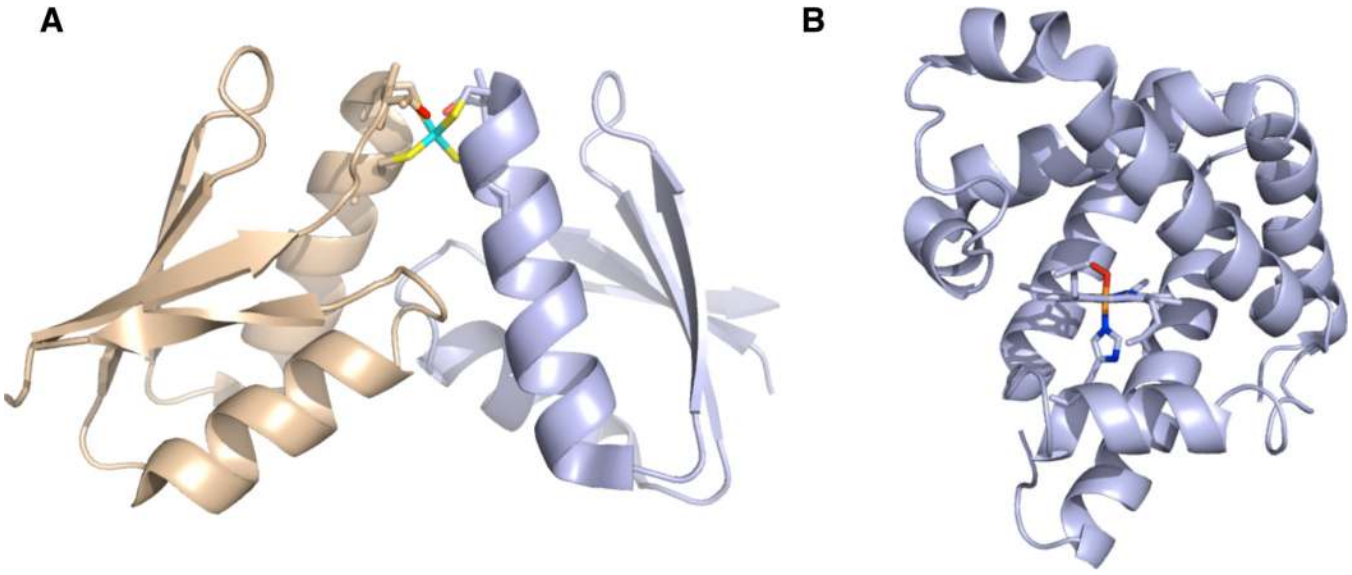

Figure 3.
Molecular structures of the homodimeric copper trafficking protein $Cu(Hah)_2$ (PDB, 1FEE) (**A**) and myoglobin (PDB, 1A6M) (**B**).

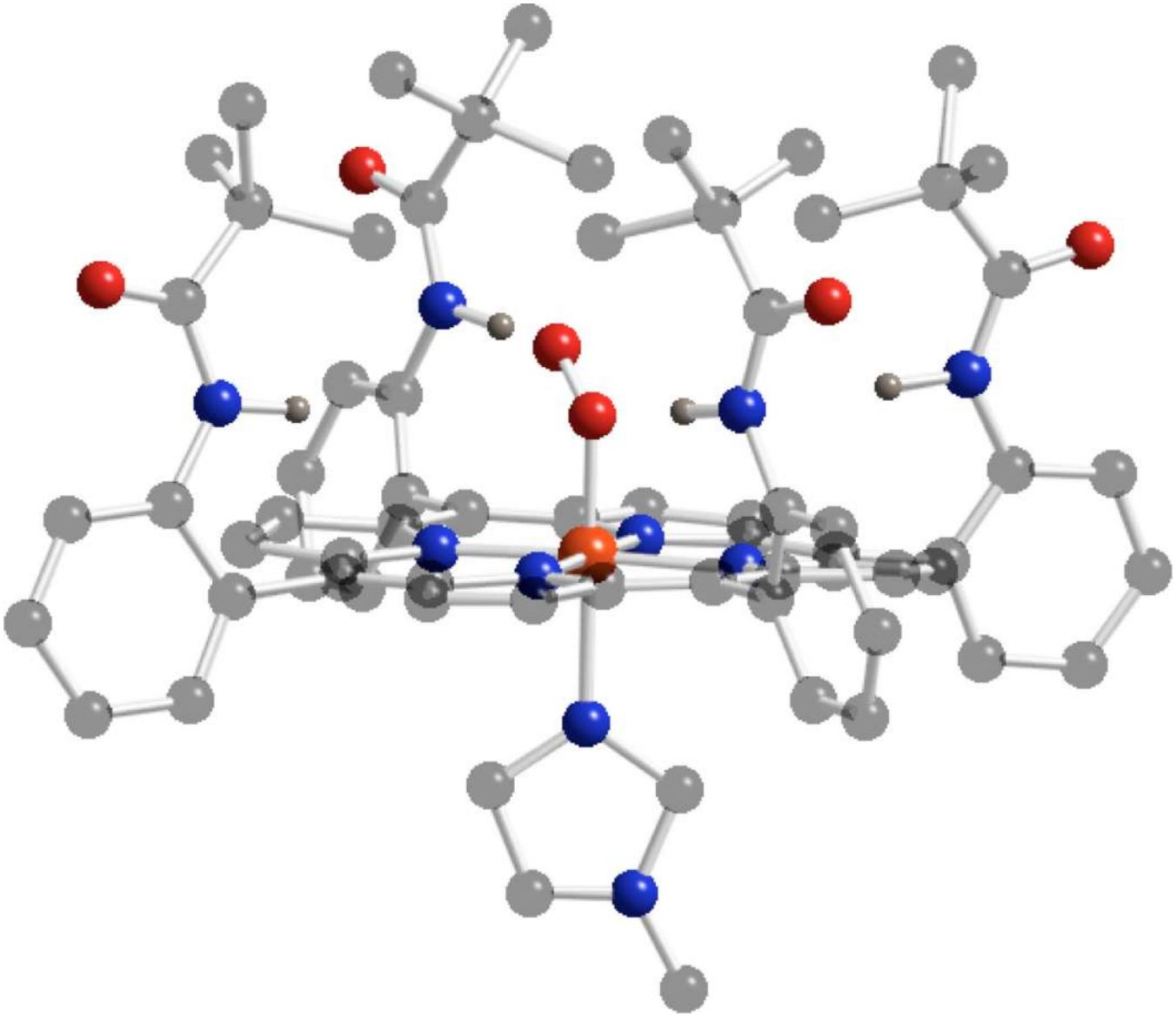

Figure 4.
Molecular structure of the Fe-O_2 picket-fence porphyrin complex.

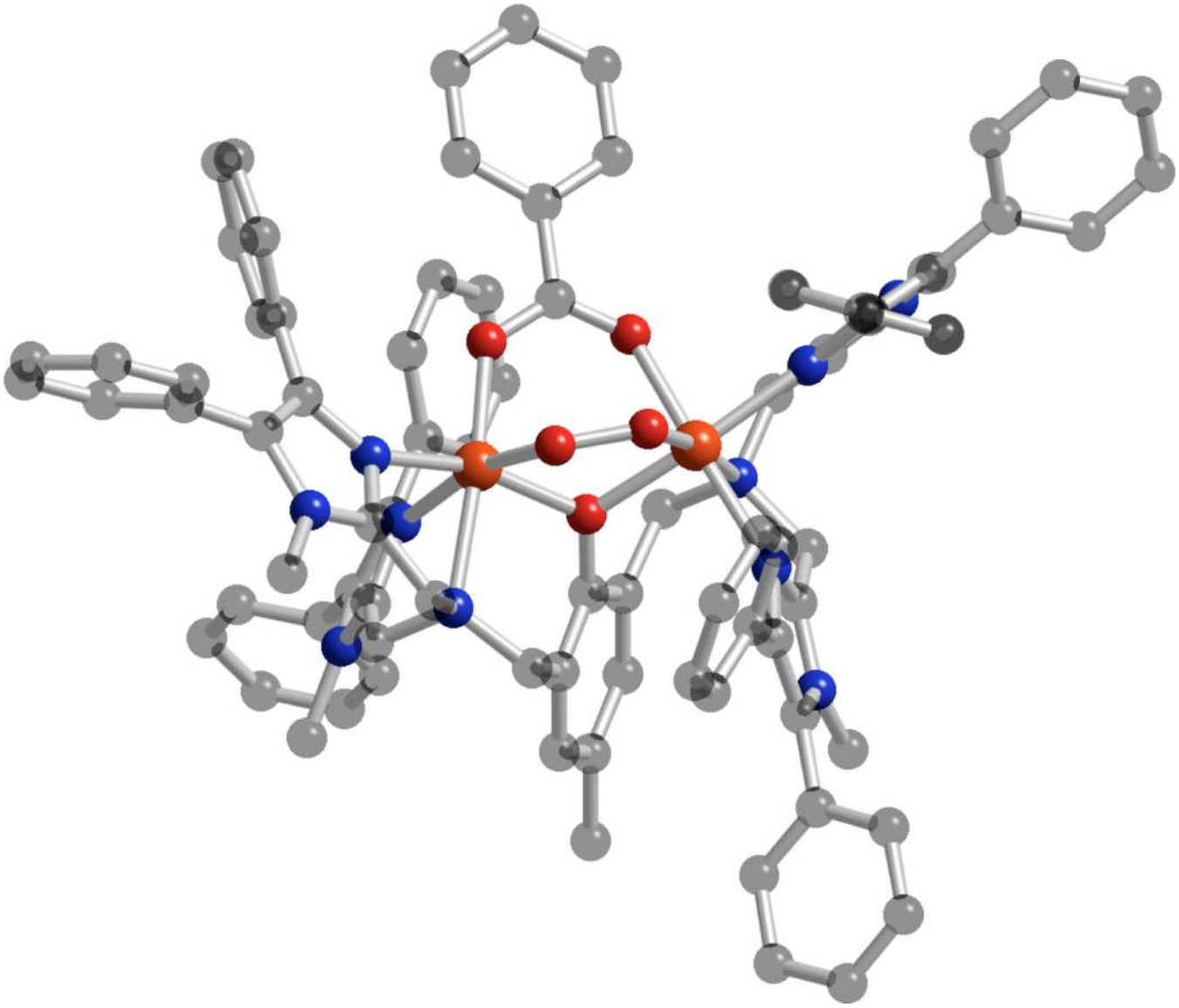

Figure 5.
Molecular structure of a Fe_2(μ-1,2-peroxo) complex containing a bulky binucleating ligand.

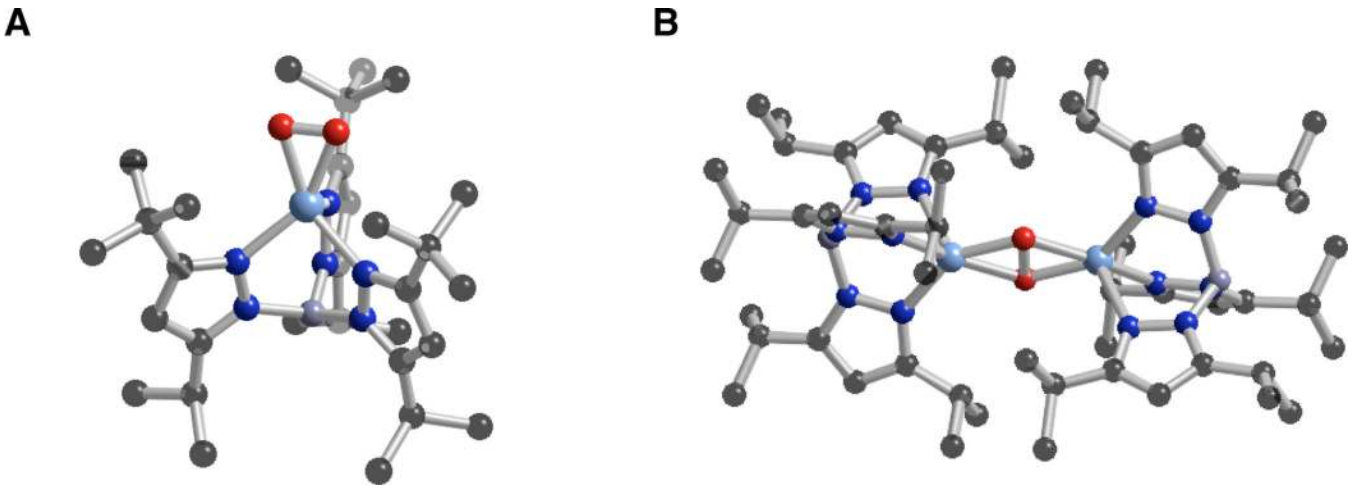

Figure 6.
Molecular structures of Cu-superoxo complex, [$CuTp^{t\text{-}Bu,iPr}(\eta^2\text{-}O_2)$] (**A**) and $\mu\text{-}\eta^2\text{:}\eta^2$-peroxo dicopper(II) complex, $[Cu^{II}Tp^{iPr,iPr}]_2(O_2)$ (**B**) showing the controlling effects of steric bulk.

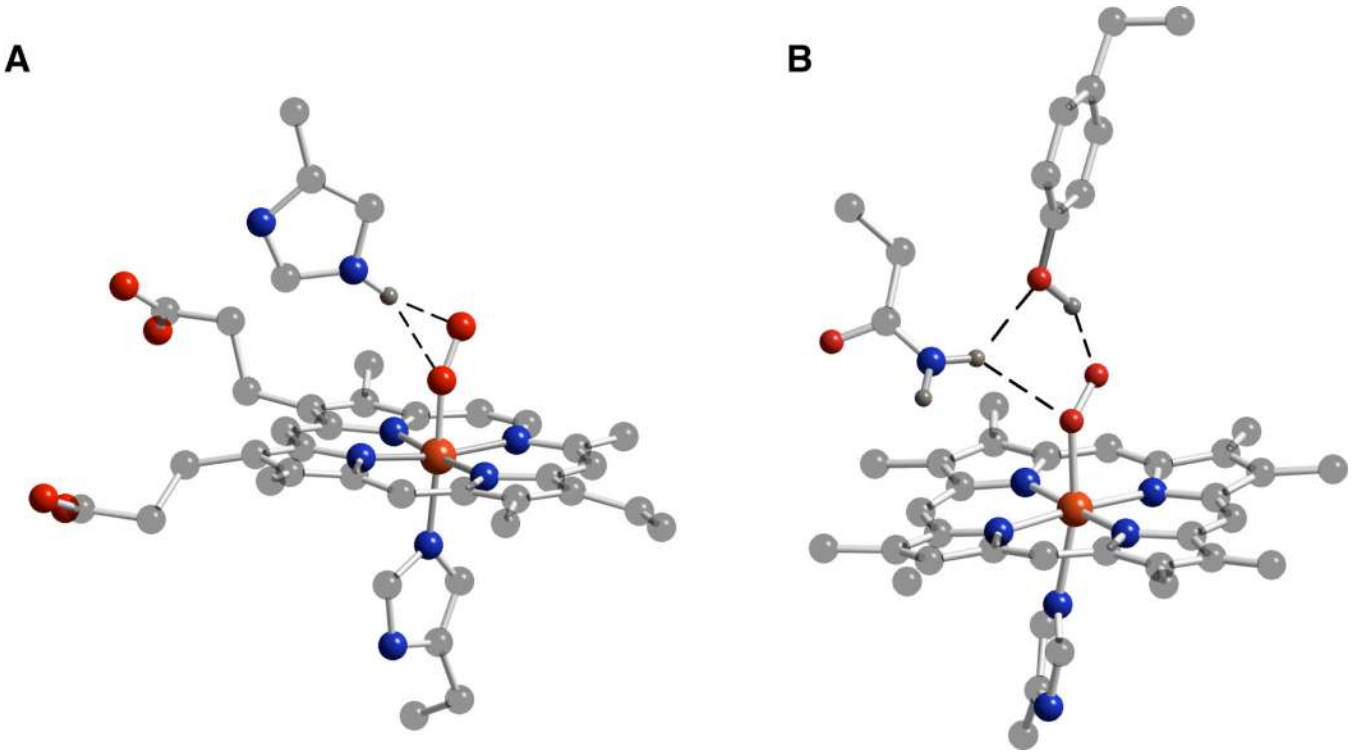

Figure 7.
Active site structures of the oxygenated forms of human hemoglobin (**A**) and nematode hemoglobin (**B**) illustrating the different H-bonding networks.

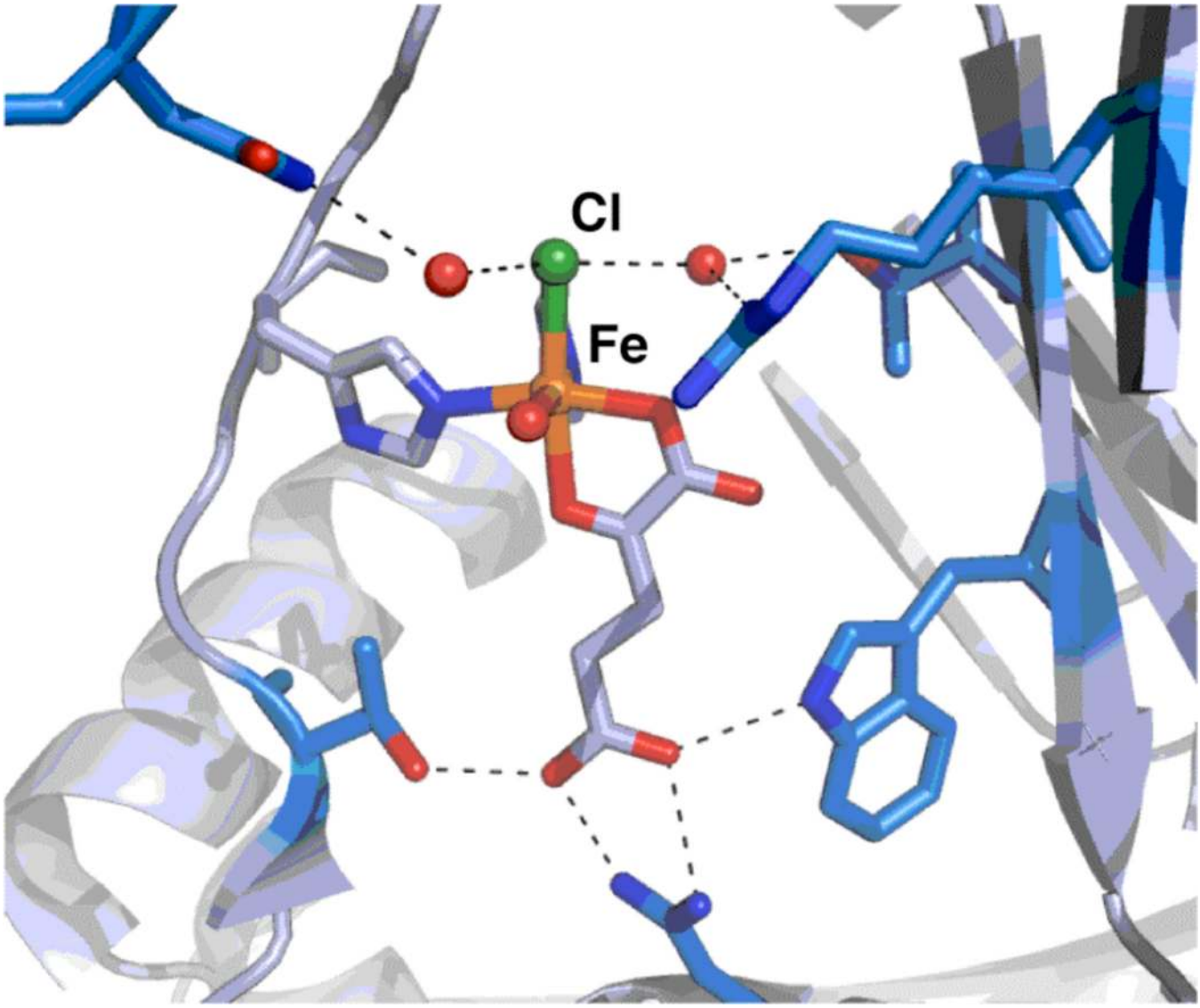

Figure 8.
Active site structure of SyrB2 showing the H-bond network surrounding the chloride ion. The red spheres represent water molecules.

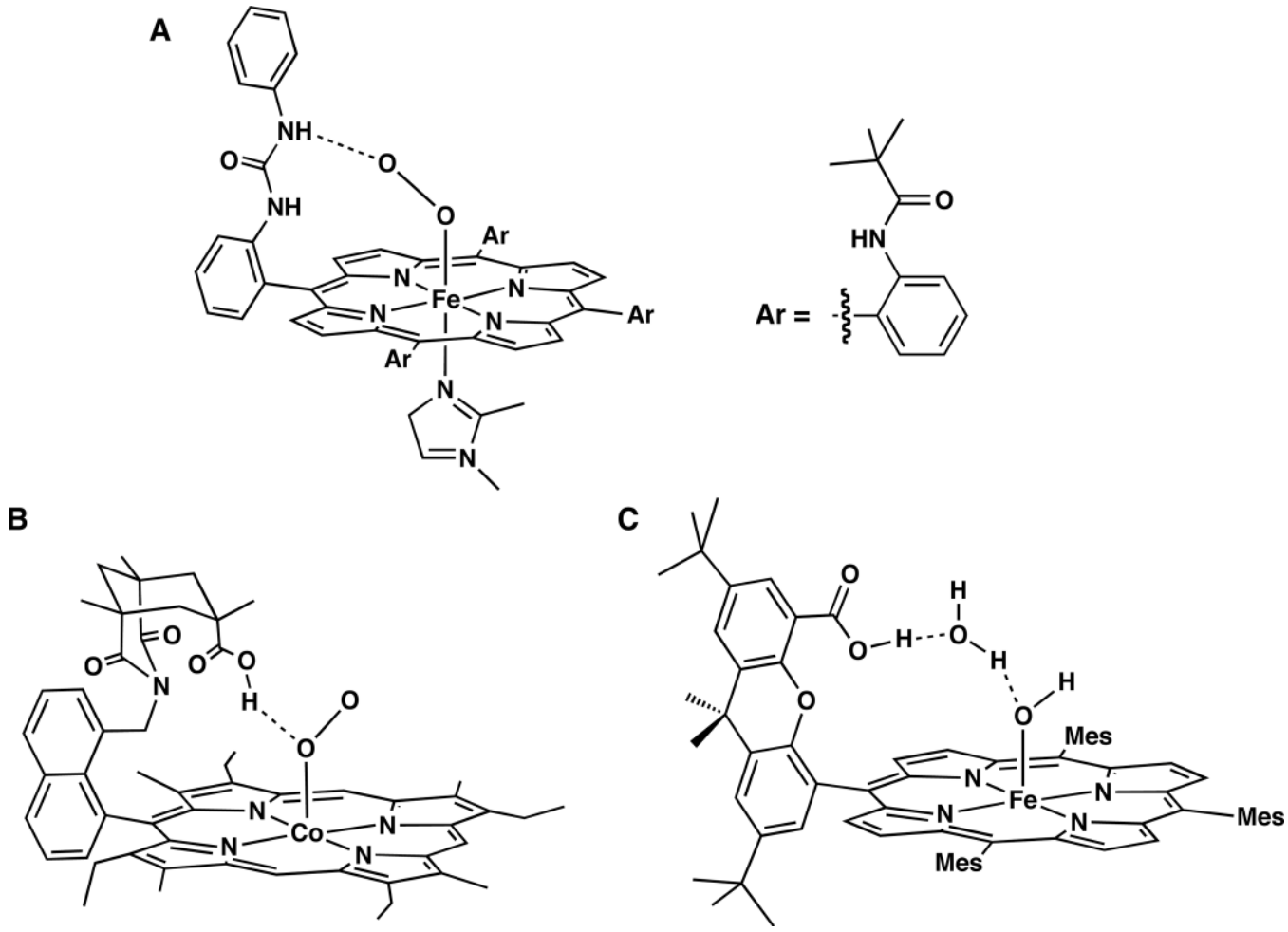

Figure 9.

H-bonding porphyrin systems: urea-modified “picket fence” porphyrin—only the urea group is shown for clarity (**A**),[28] the system developed by Change (**B**),[29] the Fe^{III}–OH "Hangman" porphyrin complex (**C**).[30]

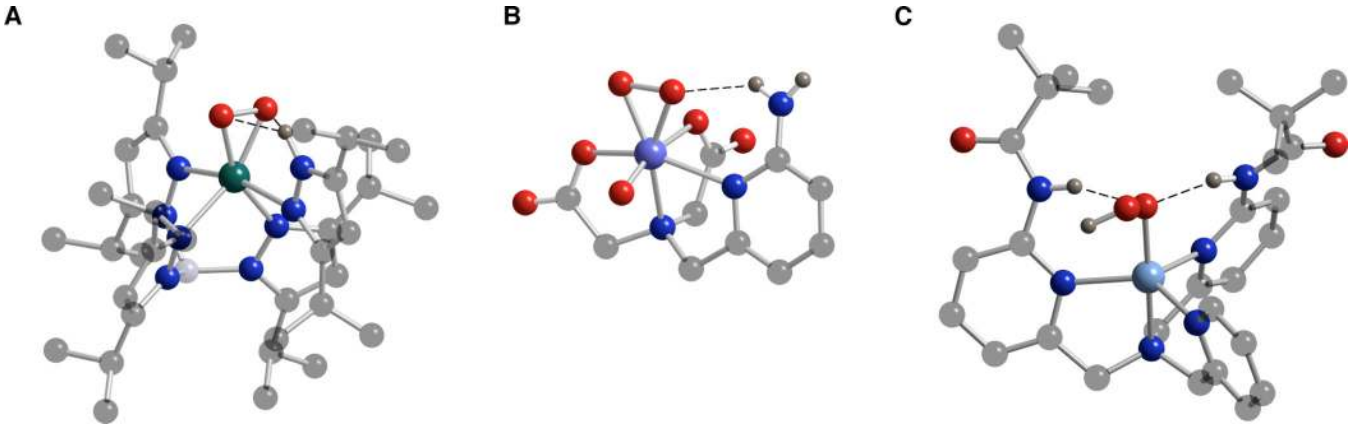

Figure 10.
Molecular structures of metal-peroxo complexes with intramolecular H-bonds: $[Mn^{III}(O_2)]$ (**A**),[33] $[V^{V}(O_2)(O)]^{-}$ (**B**),[34] and $[Cu^{II}(OOH)]^{+}$ (**C**).[35c]

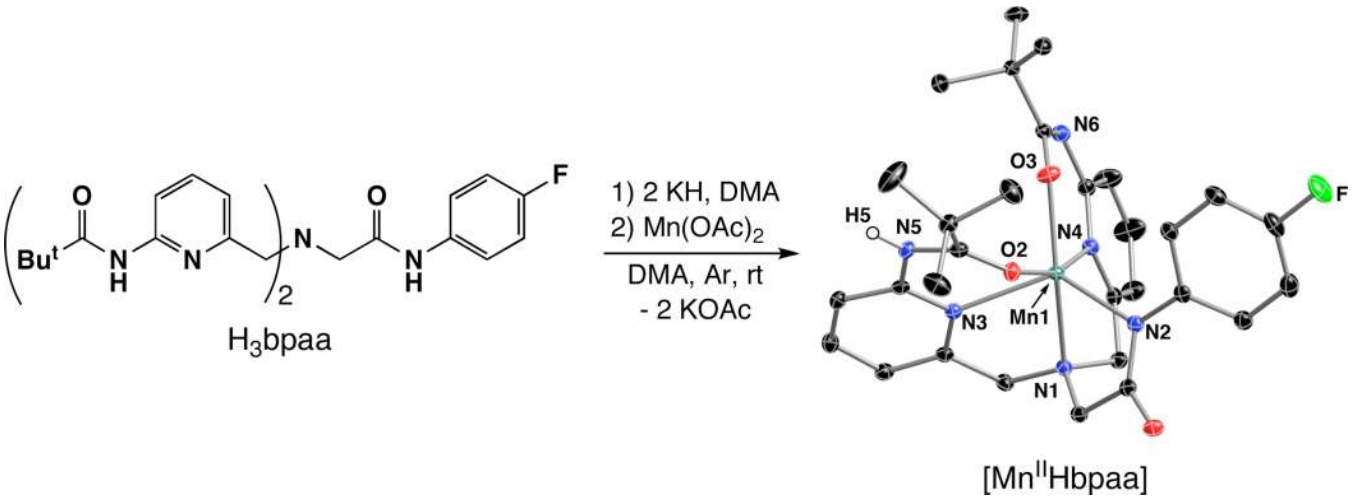

Figure 11.
Synthetic details and molecular structure for [Mn^{II}Hbpaa]. Selected distance (Å): Mn1–N1, 2.287(1), Mn1–N2, 2.157(1), Mn1–N3, 2.279(1), Mn1–N4, 2.266(2), Mn1–O2, 2.247(1), Mn1–O3, 2.047(1)

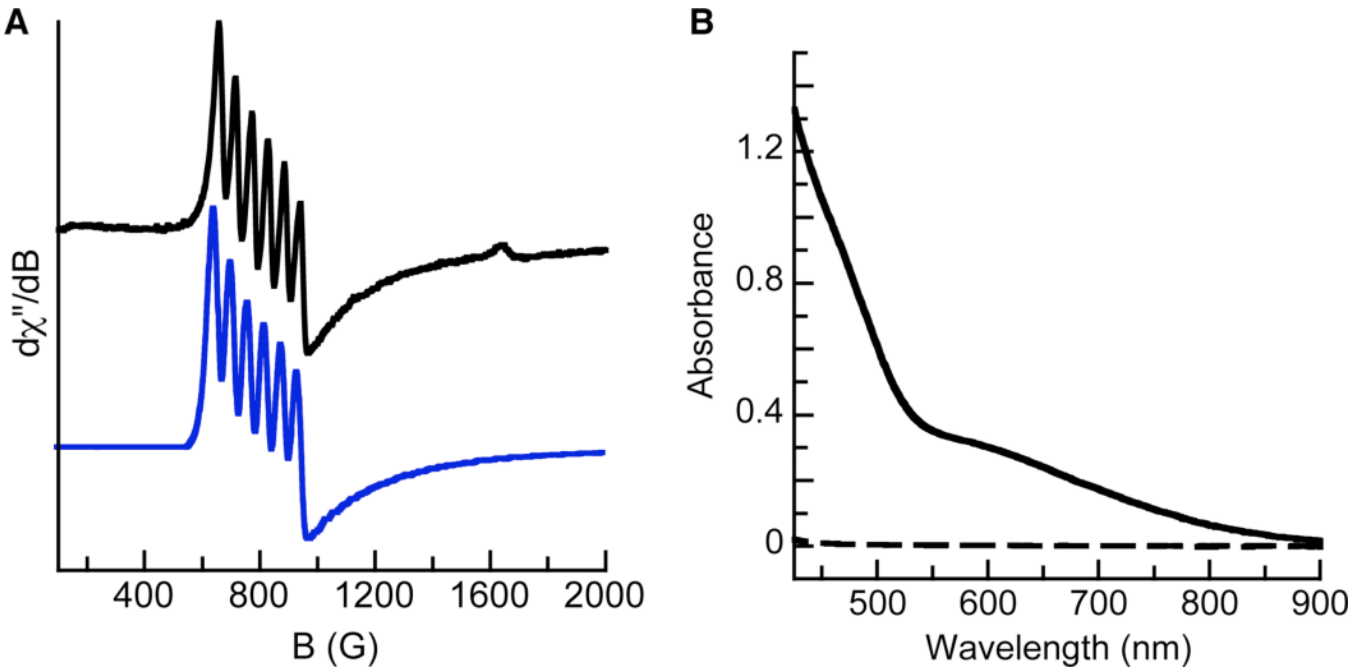

Figure 12.

Parallel-mode EPR spectrum (black) and simulation (blue) of [$Mn^{III}H_2bpaa(O_2)$] (2 mM in THF) recorded at 2.2 K (**A**) and absorbance spectra of [$Mn^{II}H_2bpaa$] (---) and [$Mn^{III}H_2bpaa(O_2)$] (—) (10 mM in DMSO) measured at room temperature (**B**). EPR parameters: Microwave frequency and power, 9.26 GHz, 0.2 mW; modulation, 10 G EPR simulation parameters: $S = 2$, $g = 2.0$, $D = -2$ cm^{-1}, $E/D = 0.13$, $A = 160$ MHz.

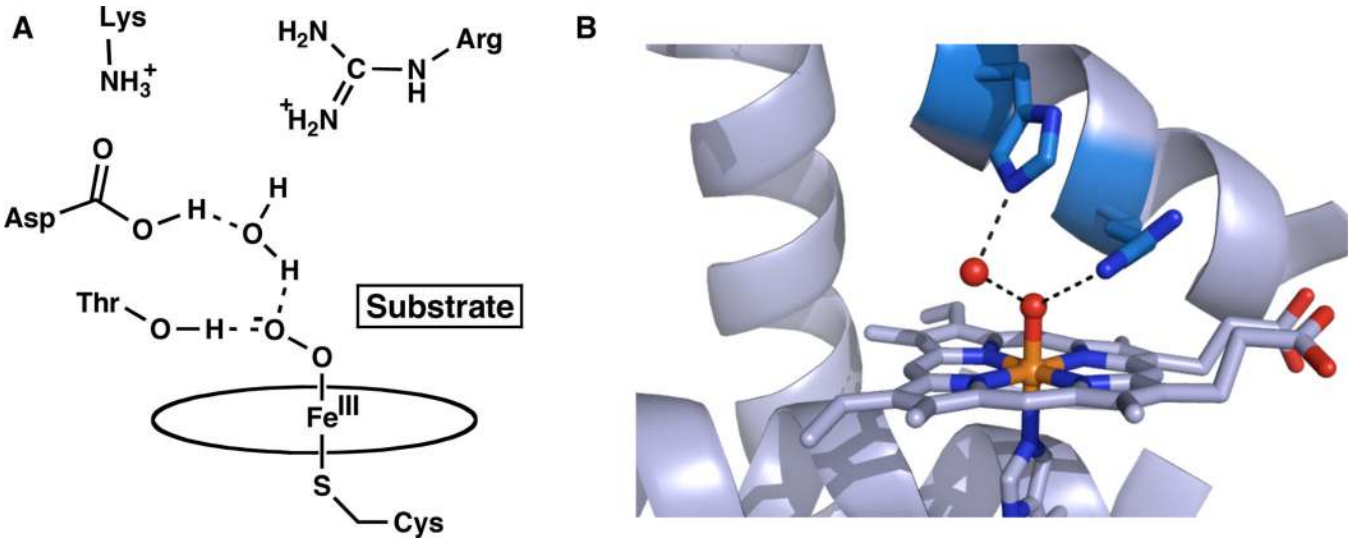

Figure 13.
The active sites of cytochrome P450 (**A**) and compound 1 of cytochrome c peroxidase (PDB, 1ZBZ) highlight the intramolecular H-bonding networks surrounding the iron centers.

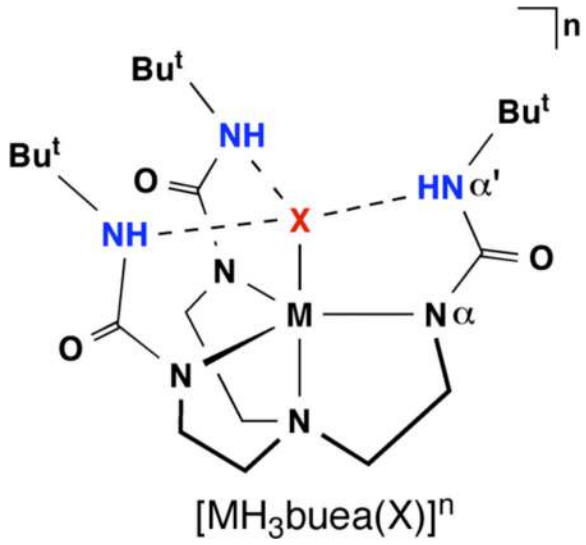

- Cavity provides up to 3 intramolecular H-bonds
- Thermodynamically favored six-membered rings are formed during H-bonding
- pK_a (α'NH) ~ 30
- Bulky R groups site isolate metal center

Figure 14.
Design criteria for complexes with the H-bonding ligand $[H_3buea]^{3-}$.

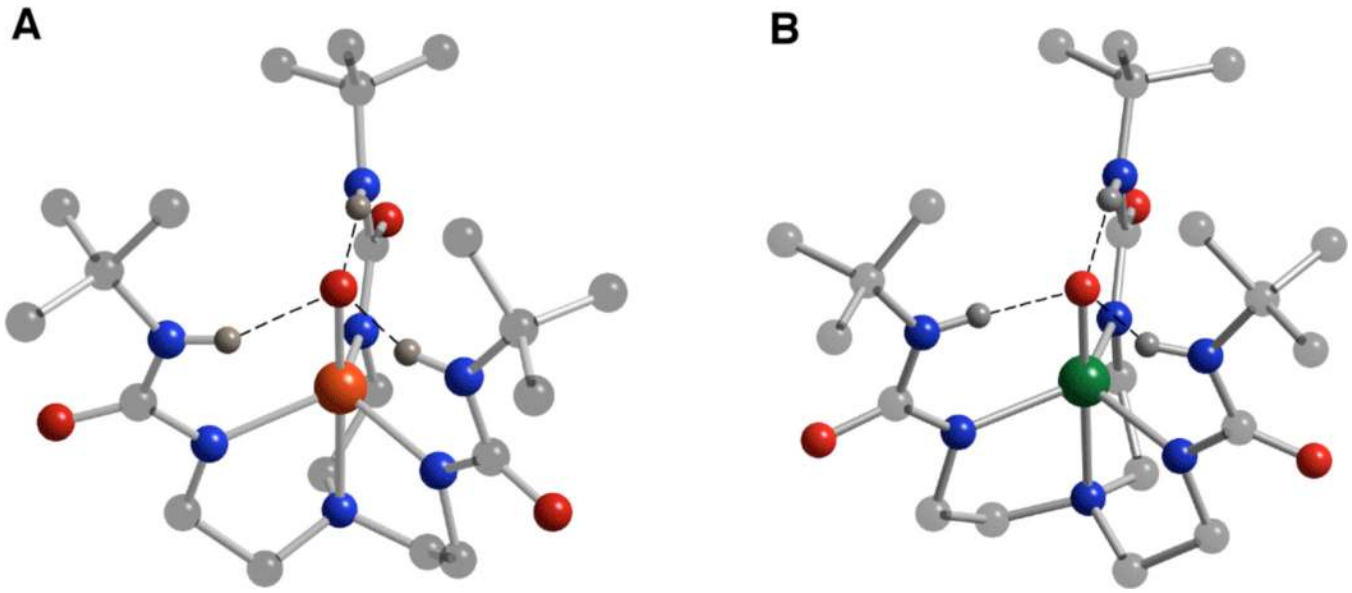

Figure 15.
Molecular structures of $[Fe^{III}H_3buea(O)]^{2-}$ (**A**) and $[Mn^{III}H_3buea(O)]^{2-}$ (**B**) determined by X-ray diffraction methods.

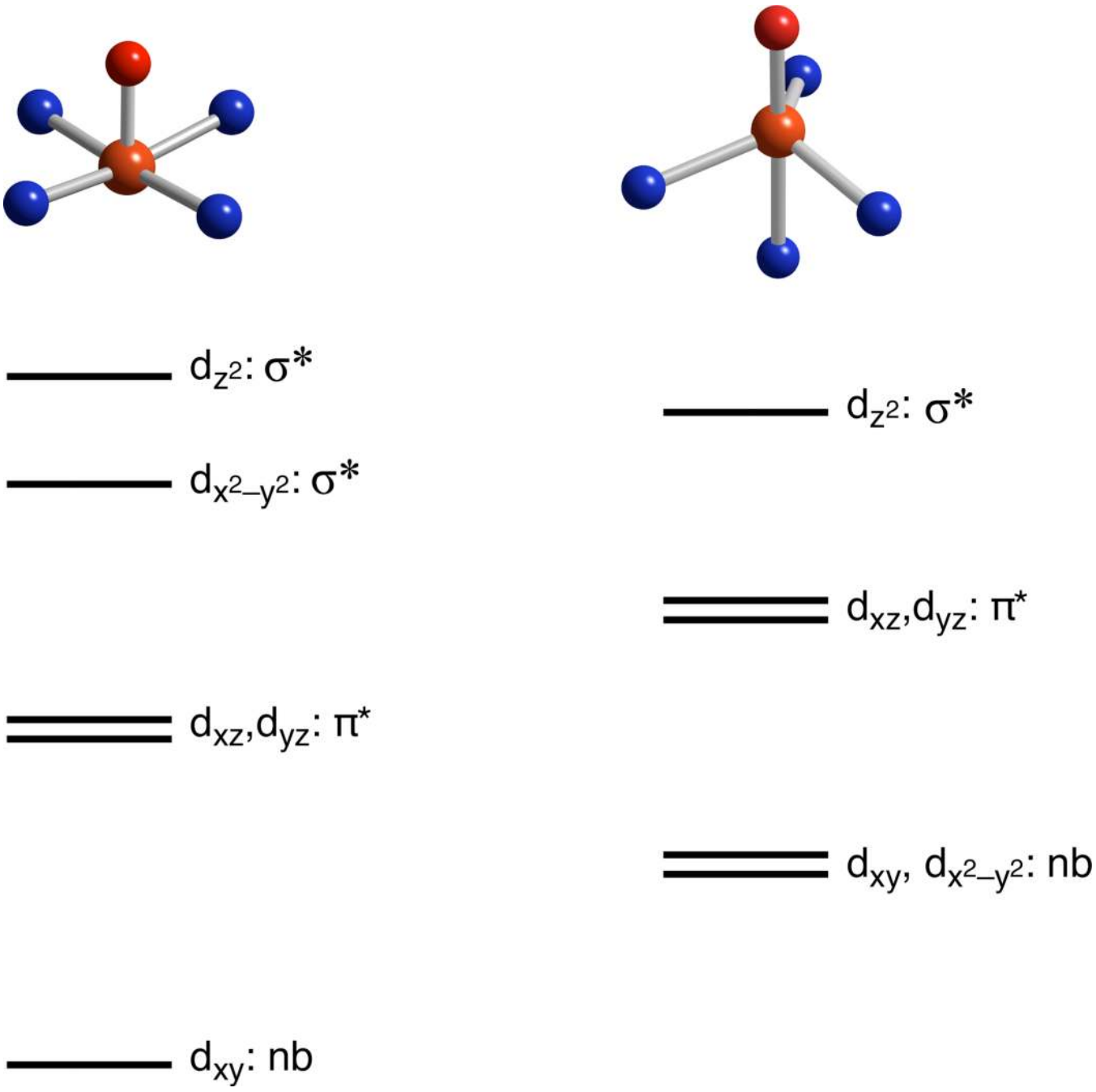

Figure 16.
Qualitative orbital diagrams for metal-oxo complexes with C_{4v} (left) and C_3 symmetry (right) (adapted from Mayer and Thorn).[48]

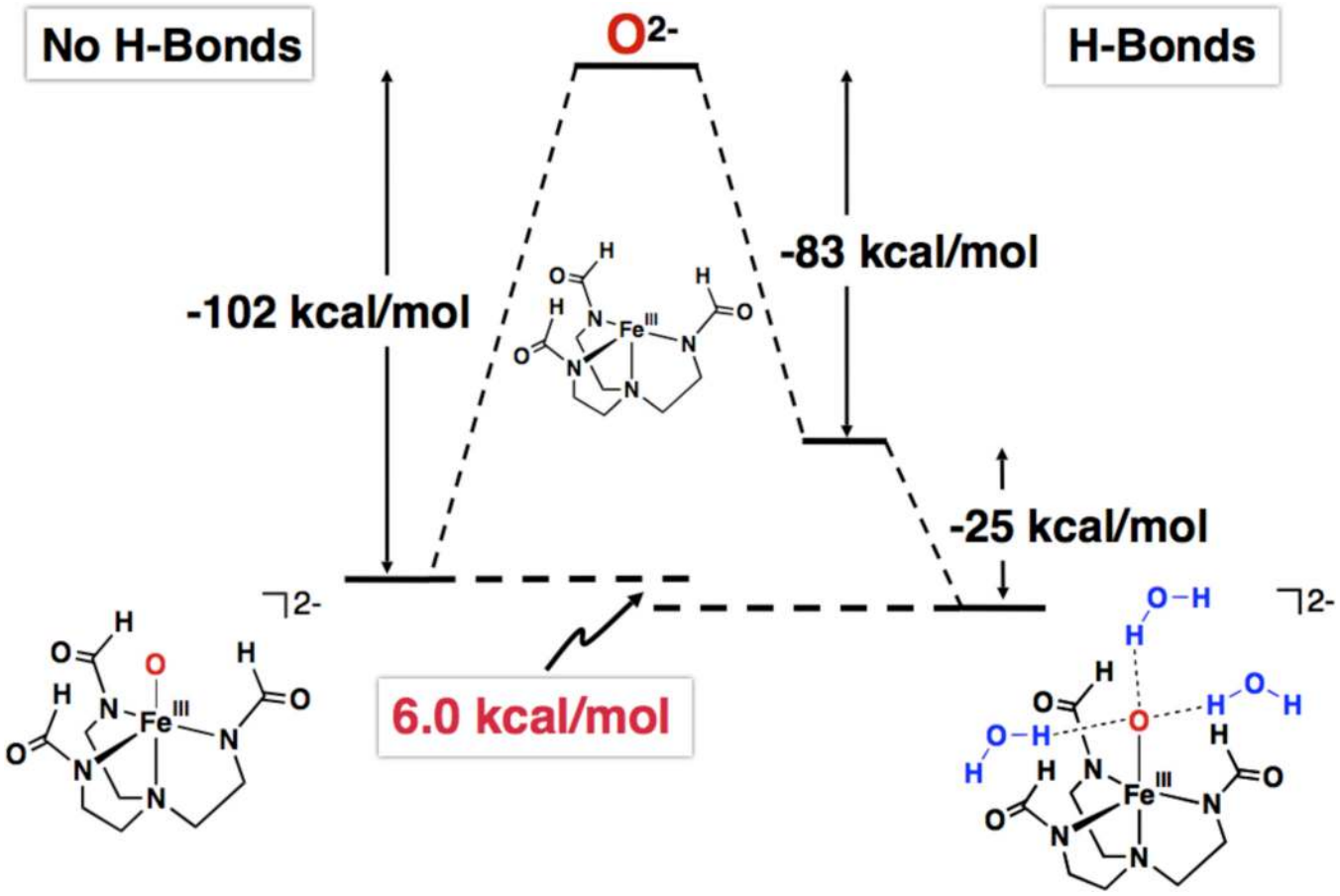

Figure 17.
Bonding decomposition scheme for the Fe^{III}–O complex illustrating the effects of the intramolecular H-bonding network.

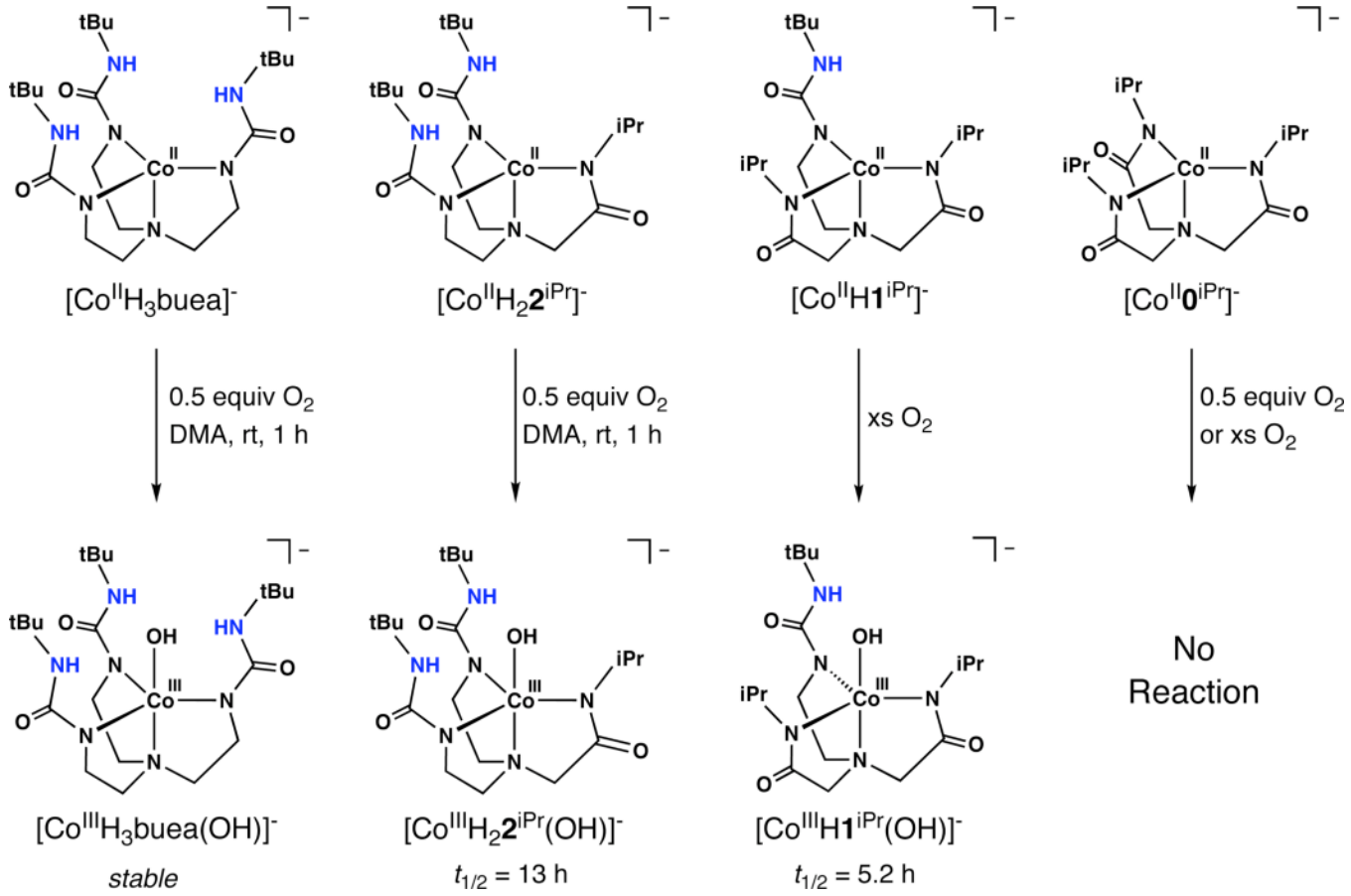

Figure 18.
Summary of the dioxygen reactivity for a series of Co^{II} complexes with varied H-bonding networks.

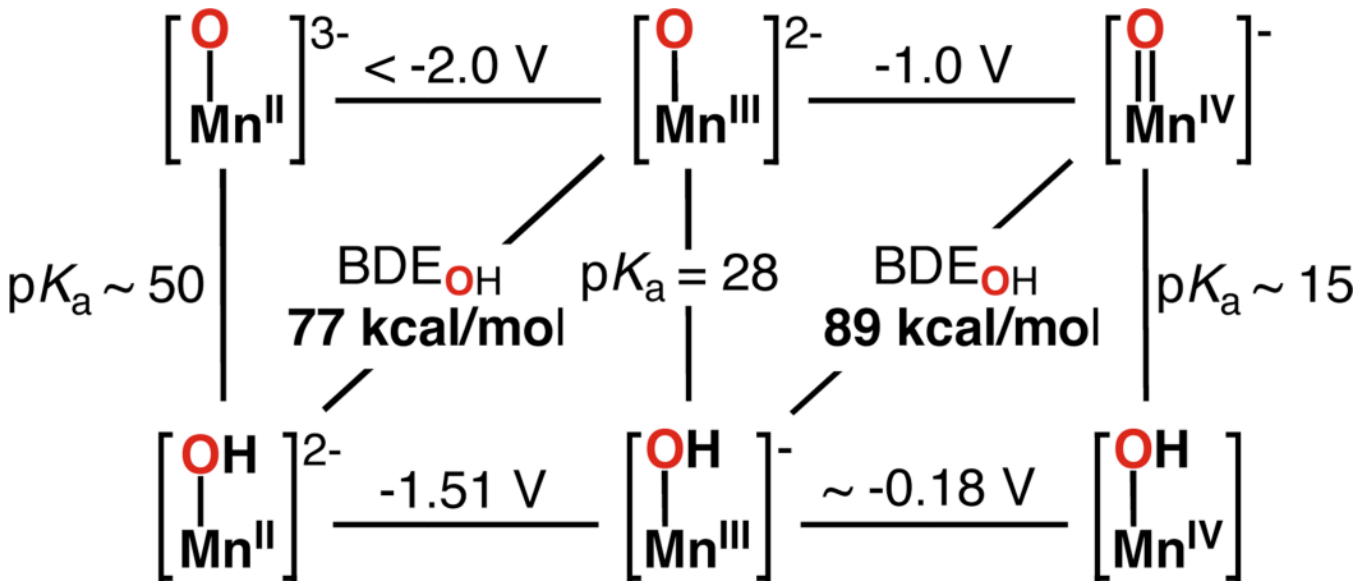

Figure 19.
Thermodynamic cycles used to evaluate the BDE_{OH} for $[Mn^{II}H_3buea(OH)]^{2-}$ and $[Mn^{III}H_3buea(OH)]^{-}$.

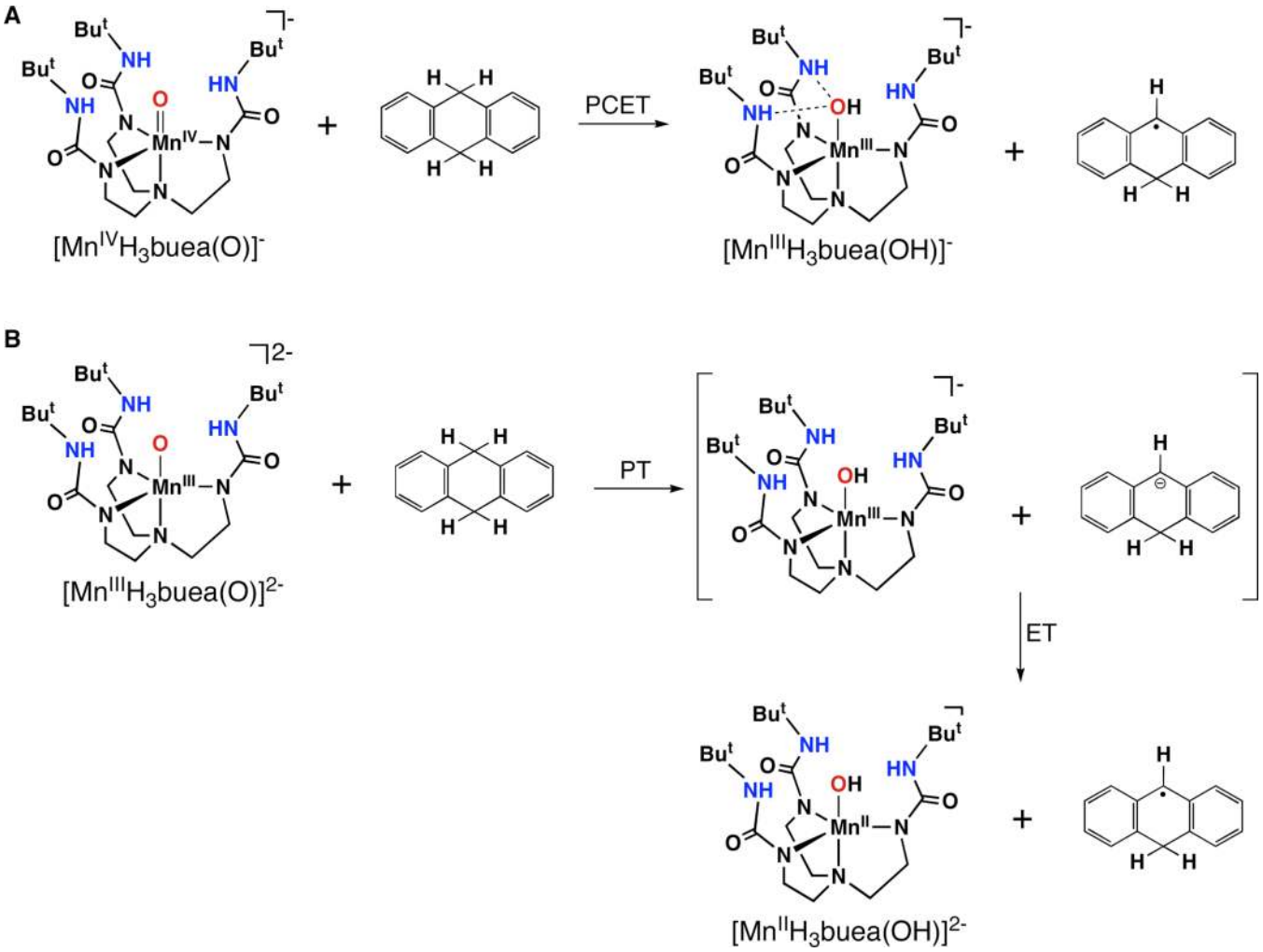

Figure 20.
Proposed mechanism for the reactions of $[Mn^{IV}H_3buea(O)]^-$ and $[Mn^{III}H_3buea(O)]^{2-}$ with DHA.

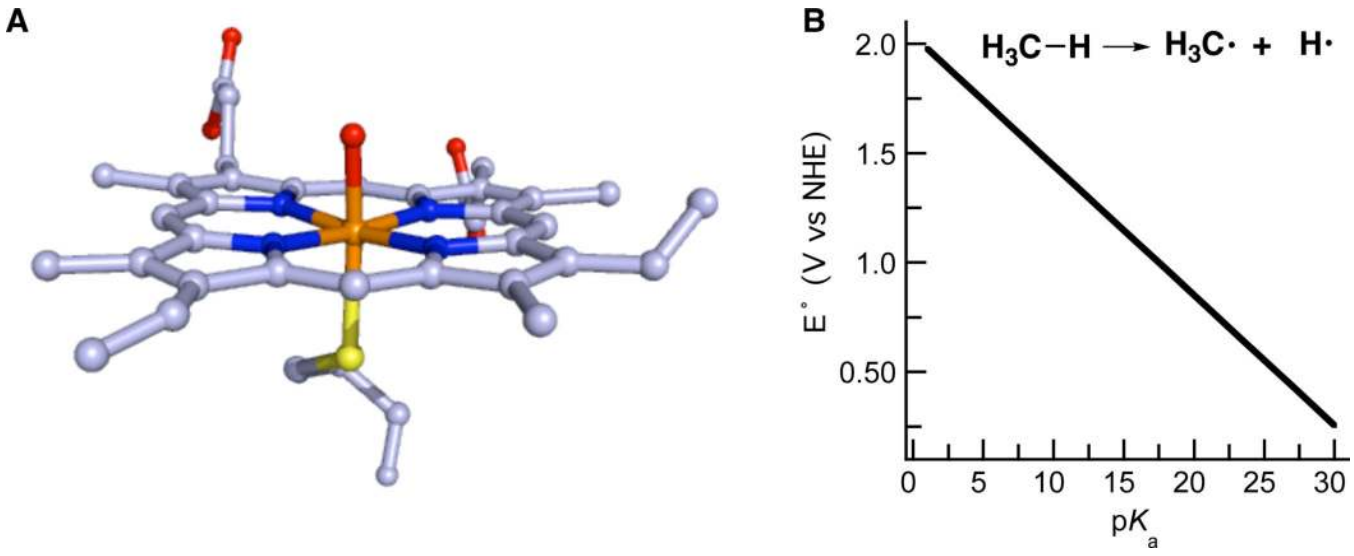

Figure 21.

Proposed structure of Compound I in cytochrome P450 (**A**) and the relationship between redox potential and pK_a for a metal-oxo species in the cleavage of a C—H bond in methane with BDE_{C-H} = 104 kcal/mol (**B**).

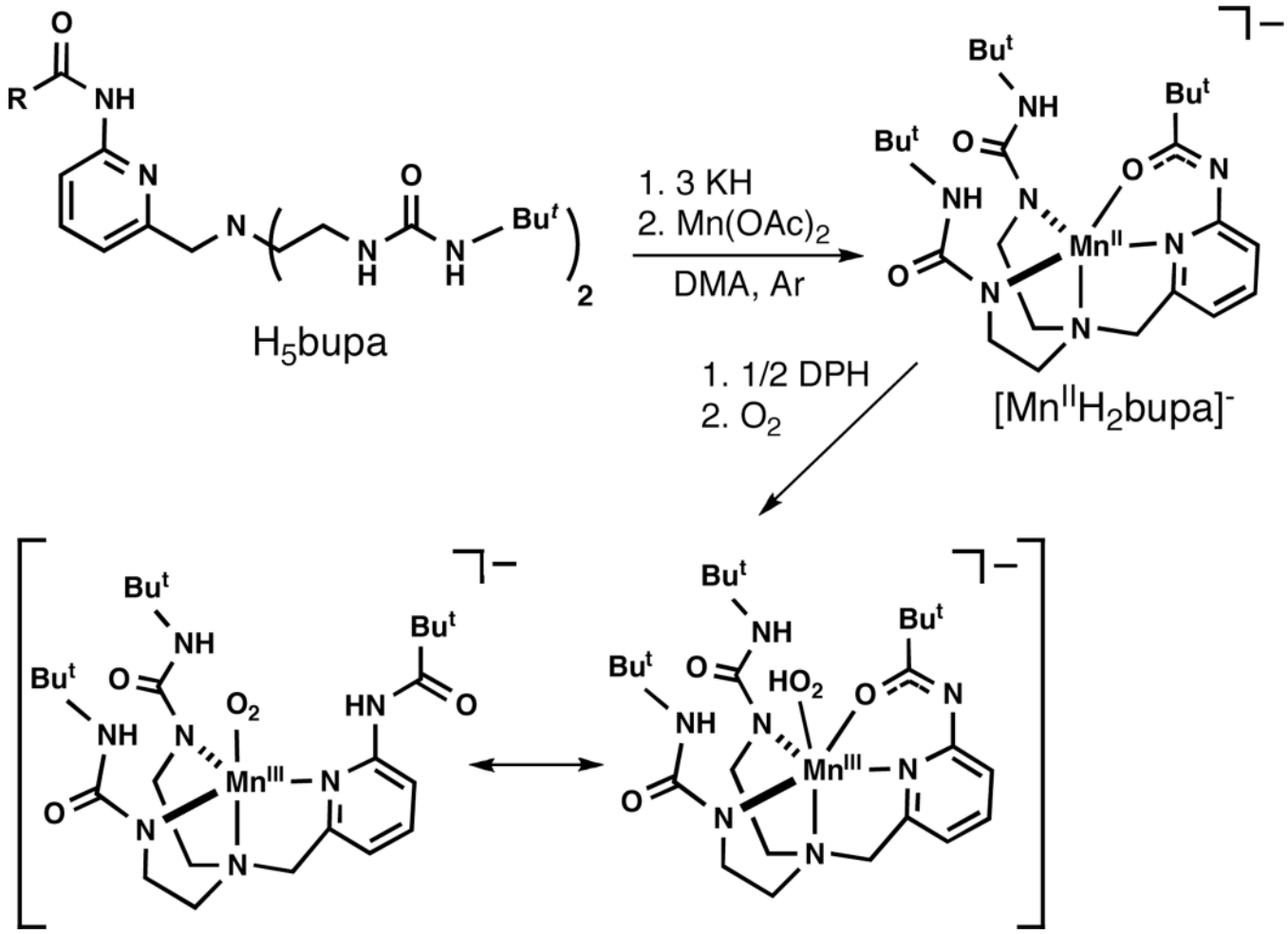

Scheme 1.

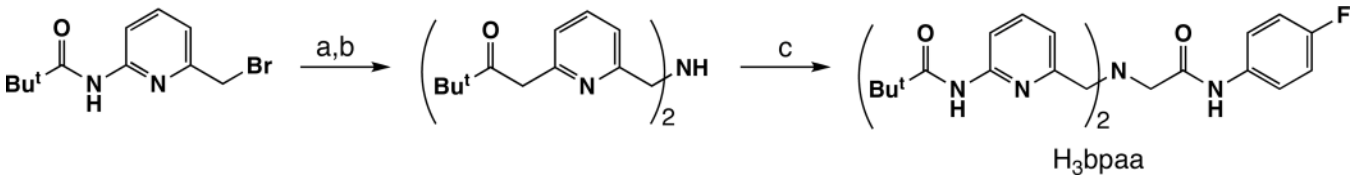

Scheme 2.

Synthetic route to the hybrid ligand, H_3bpaa. Conditions: (a) C_7H_9N, Et_3N, THF, 67°C, 76%; (b) C_6H_{10}, 20% $Pd(OH)_2$/C, EtOH, 78°C, 69%; (c) C_8H_7BrFNO, Et_3N, THF, 67°C, 92%.

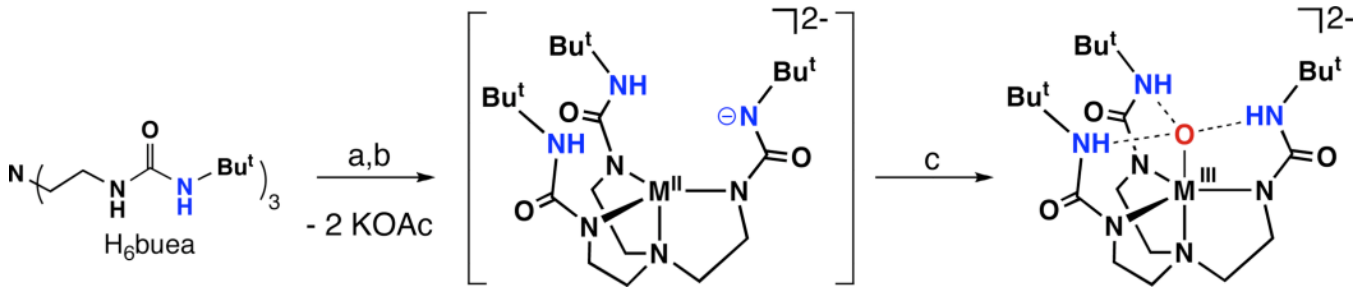

Scheme 3.

Synthetic procedure for the isolation of $[M^{III}H_3buea(O)]^{2-}$ (M^{III} = Fe, Mn). Conditions: (a) 4 KH, DMA, Ar, rt; (b) $M(OAc)_2$, DMA, Ar, rt; (c) ½ O_2, DMA, rt